PHILOSOPHICAL TRANSACTIONS OF THE ROYAL SOCIETY A MATHEMATICAL, PHYSICAL & ENGINEERING SCIENCES

The Nature of the Coordination Sites of Transition Metals in Proteins

C. David Garner, David Collison and Elna Pidcock

Phil. Trans. R. Soc. Lond. A 1996 **354**, 325-357
doi: 10.1098/rsta.1996.0011

The nature of the coordination sites of transition metals in proteins

By C. David Garner, David Collison and Elna Pidcock

Department of Chemistry, The University of Manchester, Manchester M13 9PL, UK

The nature of d-transition metal centres in proteins is considered in several respects. The results of some recent protein crystallographic studies of enzymes are described; each enzyme requires a d-transition metal atom (or atoms) for activity. The advantages of combining protein crystallography with spectroscopic studies, in particular extended X-ray absorption fine structure (EXAFS) to provide accurate interatomic distances, are discussed. Also, situations where, to date, EXAFS has been the only source of structural information are considered. The use of bond valence sum analysis and a distortional theorem to inspect the details of the geometry of a metal binding site in a protein obtained by EXAFS analysis and/or protein crystallography are advocated.

1. Introduction

'Inorganic' elements are essential for the normal development and health of all living systems. Although the majority of these element are usually only present in trace amounts, this does not diminish their significance. A considerable number of these 'trace elements' have been shown to play key roles in biological processes, including each of the d-transition metals: vanadium, manganese, iron, cobalt, nickel, copper, zinc, molybdenum and tungsten (da Silva & Williams 1991).

Crystallography is a most powerful tool capable of revealing the overall molecular architecture of proteins together with the location of an individual d-transition metal atom (or atoms) or cluster(s) of such atoms. Developments in the techniques of protein crystallization, new and more powerful X-ray sources—including the general availability of synchrotron radiation as an intense and tunable source—improved detectors, and tremendous gains in computational power for data collection and analysis, have all combined to advance significantly the applicability and precision of protein crystallography. Thus, we are moving from a situation where for (say) a metalloprotein the knowledge of a crystal structure was special to a situation where structural characterization will be achieved for several derivatives (e.g. oxidized, reduced, inhibitor) or substrate analogue-bound, site directed mutant.

This review will consider the results of some recent protein crystallographic investigations of enzymes. These have revealed vital new information concerning the nature of the d-transition metal centre (or centres) which are the site of catalytic activity. Each of the examples chosen represents a major advance in our understanding of the role of the d-transition metal (or metals) in the biochemical function of the system. Furthermore, the structural details provided for each of these metal binding sites are

Phil. Trans. R. Soc. Lond. A (1996) **354**, 325–357
Printed in Great Britain

novel and involve some important and unanticipated facet. Despite the significance of this structural information, these results should be taken to represent the beginning of a systematic investigation of the role of the d-transition metal (or metals) in the biological function of the enzyme, not the end of such a study. An important aspect of this systematic investigation is to define the coordination of the metal atom(s) and how this varies in different states of the enzyme; thus, the chemistry of transition metals is the chemistry of their complexes and we need to know the immediate and adjacent environment of metals in a protein to understand the properties of these centres. In respect of the structure of the metal site, it is important to remember that, at present, protein crystallography will not define metal–ligand distances to a precision of better than ±0.1 Å and often the resolution achieved is significantly inferior to this. Uncertainties of this magnitude can be chemically significant. Therefore, there is a clear case for using metal-edge X-ray absorption spectroscopy (XAS) to probe metal centres in proteins (Garner 1991), especially as the extended X-ray absorption fine structure (EXAFS) can provide metal–ligand bond lengths to a precision of ±0.03 Å. The combination of protein crystallography and EXAFS is particularly powerful, especially when the same state of the system is studied in each case. XAS is a versatile technique with no requirement for crystallinity and, thus, can be used independently of protein crystallograhy. This review will describe some studies where the EXAFS data are the only structural information presently available. Finally, some systematics of the coordination environment of metals in proteins will be considered using bond valence sum analysis (BVSA) (Brown & Altermatt 1985) and distortional theorem (Brown & Shannon 1973) approaches.

2. Protein crystallographic investigations

(a) *Isopenicillin N synthase*

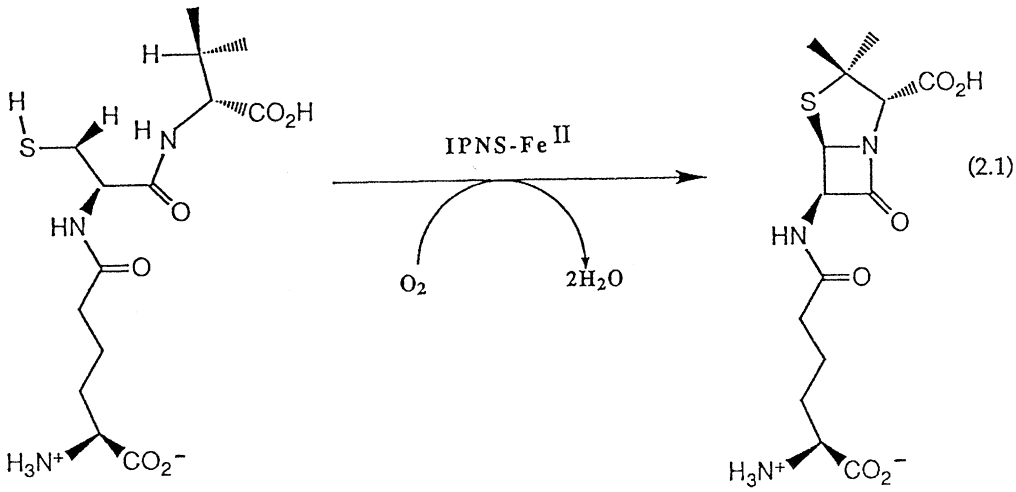

(2.1)

The key step in penicillin biosynthesis (2.1), in which both the β-lactam and thiazolidine rings of the nucleus are created, is mediated by isopenicillin N synthase (IPNS), which binds Fe^{II} and uses dioxygen as a cosubstrate. In a unique enzymatic step, with no chemical precedent, IPNS catalyses the transfer of four hydrogen atoms from its tripeptide substrate to dioxygen forming, in a single reaction, the complete bicyclic nucleus of the penicillins (Pang *et al.* 1984).

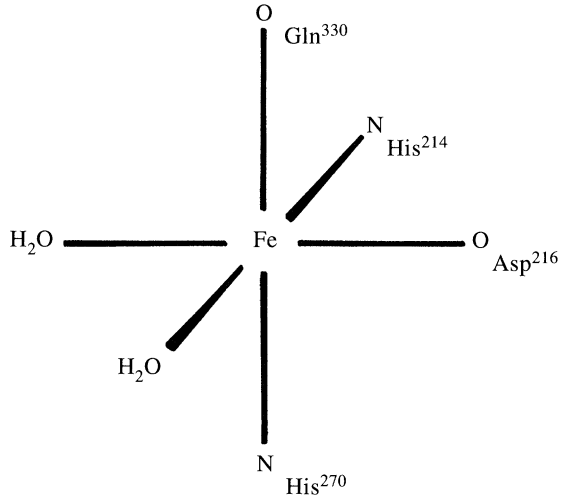

Figure 1. Representation of the coordination of the Fe^{II} site of isopenicillin N synthase from *Aspergillus nidulans* based on the structure of the manganese derivative (Roach *et al.* 1995).

The structure of IPNS from a recombinant *Aspergillus nidulans* containing manganese has been determined at a resolution of 2.5 Å (Roach *et al.* 1995). The catalytically active site is unusually buried within a 'jelly roll' motif and lined by hydrophobic residues. Figure 1 shows the coordination environment proposed for Fe^{II} on the basis of the results obtained for the manganese derivative, although it must be remembered that the protein environment may be peculiar to the particular metal bound. The Fe^{II} centre is labile and considered to bind O_2 in place of Gln^{330} and since Fe *K*-edge EXAFS (Randall *et al.* 1993) indicates coordination of the sulphur of the tripeptide, this ligation is suggested to occur in place of the H_2O molecule *trans* to Asp^{216}. A detailed mechanism for the catalysis (2.1) has been proposed (Roach *et al.* 1995), whereby dioxygen utilizes its full, four-electron, oxidizing power. Amino acid sequence comparisons between IPNS, 1-aminocyclopropane-1-carboxylic acid oxidase and some 2-oxo-acid-dependent oxidases indicate that they contain a conserved 'jelly roll' motif and form a structural family of enzymes. This conservation of structural and active-site motifs throughout a number of these enzymes suggests that they operate by closely related mechanisms. Gln^{330} is conserved through all IPNS sequences but is not conserved through other members of the family. This difference in coordination chemistry presumably reflects differences in their mechanism and substrate specificity, in particular the fact that IPNS does not use a 2-oxo-acid cosubstrate.

(*b*) *Amine Oxidase from Escherichia coli*

Amine oxidases are regulatory enzymes which catalyse the oxidation of a wide range of biogenic amines such as histamine and neurotransmitters. The copper-containing amine oxides have been well studied by spectroscopic and kinetic methods (Klinman & Mu 1994) and comprise one copper atom and one organic cofactor per subunit. The cofactor was initially proposed to be 2,7,9-tricarboxypyrroloquinoline quinone (PQQ) (Duine & Jongejan 1989) but was later identified to be the quinone derived from 2,4,5-trihydroxyphenylalanine (TPQ) in bovine serum amine oxidase (Janes *et al.* 1990) and in other copper amine oxidases (Mu *et al.* 1992).

The structure of the amine oxidase from *Escherichia coli* has been solved at 2.0 Å resolution (Parsons *et al.* 1995). The dimeric protein of 725 amino acids has an

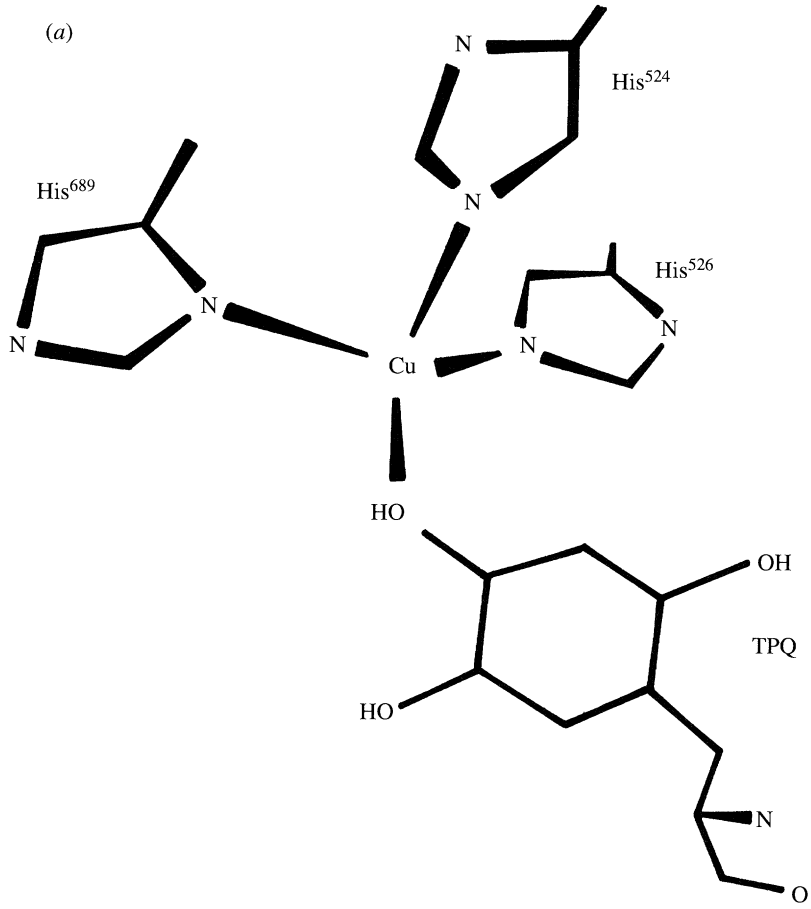

Figure 2. Representation of the structure of the copper site of amine oxidase from *Escherichia coli*: (*a*) inactive form. (Parsons *et al.* 1995).

active site at the dimer interface which is buried away from solvent. Two forms have been crystallized: an inactive form (grown from ammonium sulphate) and an active form (grown from sodium citrate solutions) and, crucially, the only difference in the molecular structure of these two forms occurs at the copper site. In the inactive form the copper site (figure 2*a*) comprises three imidazole N atoms from histidine residues, 524, 526 and 689 (two Nε and one Nδ), and an oxygen atom from the four-position of a TPQ cofactor. There are no water molecules bonded directly to the copper. The coordination at copper is a trigonal pyramidal distortion of a tetrahedron, with the His^{524} nitrogen atom in the 'axial' position. The average bond lengths over the two subunits have $Cu{-}N_{eq}$ 1.94 Å, $Cu{-}O_{TPQ}$ 2.11 Å and $Cu{-}N_{ax}$ 2.18 Å. This trigonal pyramidal geometry can be compared to that found for the copper site in nitrite reductase from *Achromobacter cycloclastes* (Godden *et al.* 1991), where three Nε histidine ligands form the basal plane and a water molecule is the axial ligand.

The structure of the active form of the enzyme has been refined to 2.4 Å resolution and shows that the copper atom is five-coordinate, binding the three histidine N atoms, as found for the inactive form, plus two water molecules (figure 2*b*).

This coordination geometry is best described as a distorted square pyramid, with

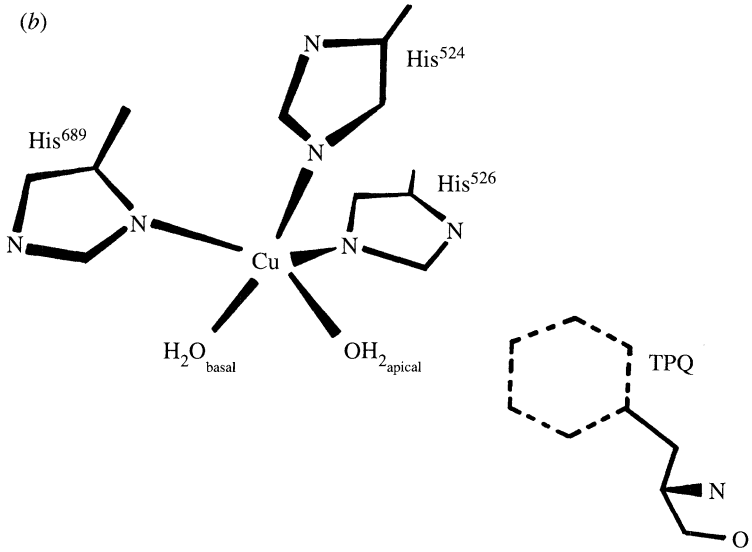

Figure 2. (*b*) Active form (Parsons *et al.* 1995).

a water molecule as the apical ligand at 2.7 Å distant from the copper atom; the four ligand atoms in the basal plane are between 2.0 and 2.1 Å away from the copper. The copper atom and all three histidine ligands are almost superimposable in position between the two crystal forms. It is satisfying to note that, prior to this crystal structure determination, detailed spectroscopic studies of amine oxidases had suggested that the active site comprised three histidine ligands together with one basal and one apical water molecule. Thus, in the active form of the enzyme, the TPQ is not coordinated to the copper atom and lies closer to a basic residue of asparagine, which has been postulated to take part in catalysis (Farnum *et al.* 1986). Unfortunately, the structure of the active form of the enzyme is not of a sufficiently high resolution to reveal the ring orientation of TPQ nor the details of its interactions with other groups. Nonetheless, this study has provided further evidence that changes in geometry and coordination number of the copper site in type-II copper proteins can have profound effects for reactivity. This highlights the need to perform complementary diffraction and spectroscopic measurements on metalloproteins.

(*c*) *Aldehyde ferredoxin oxidoreductase from Pyrococcus furiosus*

Molybdenum and tungsten are the only second and third row d-transition metals with established biological roles (Stiefel *et al.* 1993). These elements are now known to be stoichiometric constituents of several enzymes within the carbon, nitrogen or sulphur cycles and, with the notable exception of the nitrogenases, all of the enzymes can be classified as oxotransferases. The catalysis involves the transfer of an oxo group to or from a substrate in a two-electron redox reaction, e.g. $SO_3^{2-} \rightarrow SO_4^{2-}$, sulphite oxidase; $RCHO \rightarrow RCO_2H$, aldehyde oxidase; $NO_3^- \rightarrow NO_2^-$, nitrate reductase. Tungsten enzymes (Adams 1994) (tunzymes) have, so far, been found mainly in thermophilic anaerobes and either activate CO_2 or convert aldehydes to carboxylic acids. The catalytic site in these enzymes is labile and dioxygen sensitive and comprises the metal bound to an organic cofactor. The organic ligand is termed molybdopterin (MPT) and was first identified from oxomolybdoenzymes using organic degradative techniques in conjunction with fluorescence and mass spectroscopy (Rajagopalan

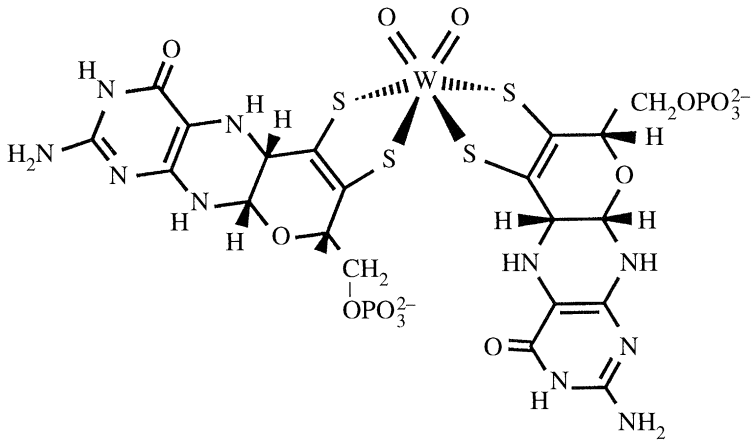

Figure 3. Representation of the structure of the tungsten cofactor of aldehyde ferredoxin oxidoreductase from *Pyrococccus furiosus* which contains two molybdopterins (see Chan *et al.* 1995).

1991). All eukaryotic molybdoenzymes contain the unmodified MPT, but prokaryotic enzymes usually contain a nucleotide bound through pyrophosphate (Johnson *et al.* 1990; Karrasch *et al.* 1990), although the role of this nucleotide is unknown. The proposed structure for the molybdenum cofactor MOCO entails a single MPT bound to molybdenum through a 1,2-dithiolato (dithiolene) group. This sulphur ligation is consistent with EPR and EXAFS spectroscopic studies (Bray 1988; Garner 1991); the latter technique unambiguously identifies terminal oxo groups on molybdenum.

All tunzymes contain either MPT or a modified MPT. The first X-ray diffraction study which established the structure of the MPT has been obtained for the tunzyme *Pyrococcus furiosus* aldehyde ferredoxin oxidoreductase for crystals obtained under anaerobic reducing conditions and solved at 2.3 Å resolution (Chan *et al.* 1995). The identity of the MPT and its mode of ligation to the metal (figure 3) confirms the excellent and insightful work of Rajagopalan (1991).

However, there are two surprising aspects. First, there are *two* of these organic moieties per tungsten, each bound through a dithiolene group. Second, the organic framework is tricyclic; the third ring is formed by cyclization of a side chain hydroxyl group with the pterin ring at C-7. The pterin ring system is non-planar and this suggests reduction to possibly a 5,6-dihydropterin. The tungsten and sulphur atoms are in a distorted square pyramidal arrangement and the angle between the planes of the MPTs is *ca.* 97°. There are no protein ligands bound to the tungsten. Further consideration of the residual electron density around the tungsten suggests that there may be two additional ligands, either chelating glycerol (from the buffer) or oxo ligands. The inclusion of oxo ligands would be consistent with EXAFS studies (George *et al.* 1992). It is suggested that the overall coordination geometry at the tungsten is that of a distorted trigonal prism. The carboxylate and imidazole side chains of a glutamate and a histidine residue are close to the oxo site(s) of the tungsten and may participate in proton transfers associated with the redox reactions. The two MPT ligands are also linked to each other through their phosphate groups, which coordinate to the axial sites of a Mg^{2+} ion. Octahedral geometry of Mg^{2+} is completed with a pair of *cis* water molecules directed towards the tungsten atom and a pair of carboxyl oxygen atoms, from asparagine and alanine residues, remote from the tungsten. The water molecules are each within hydrogen bonding distance

of a phosphate oxygen atom, the N-5 nitrogen atom of the pterin ring, and one water molecule also hydrogen bonds to the ether oxygen atom of one MPT.

The aldehyde ferredoxin oxidoreductase molecule consists of two identical 605 residue (66 kDa) subunits. A single metal atom, tentatively identified as iron, found at the dimer interface, is in a tetrahedral environment formed by one glutamate carboxylate oxygen atom and one histidine nitrogen atom from each subunit. The identification of the metal was based on anomalous scattering of the atom and this centre is thought to play a structural rather than a redox role because it is located 25 Å from the nearest tungsten centre. An (Fe_4S_4) cluster is positioned *ca.* 10 Å from the tungsten atom. The proximity of the cluster to a paramagnetic centre had already been indicated using EPR, MCD and resonance Raman spectroscopies. Four cysteinyl sulphur atoms complete the four coordination of the iron atoms in the usual way, but the polypeptide sequence around one of these cysteine residues is distinct from that normally adopted in four-iron ferredoxins. There are two hydrogen bonding routes linking the [Fe_4S_4] cluster to one of the MPT ligands.

(*d*) B_{12} *Bound to methionine synthase*

The solution of the crystal structure of vitamin B_{12} was one of many outstanding successes for Dorothy Hodgkin (1956). The structures of adenosylcobalamin and methyl cobalamin are also known. The total synthesis of these molecules, as well as the cloning, sequencing and expression of all of the genes of B_{12} biosynthesis, have been achieved. Cobalamin-dependent enzymes are involved in biological organometallic chemistry and catalyse reactions which are difficult to initiate and/or control, such as carbon skeleton rearrangements or the removal of a methyl group from a tertiary amine. The chemistry which is central to the cobalamin prosthetic group is the formation of a cobalt–carbon bond, linking cobalt to a methyl group in methylcobalamin (figure 4) to a cyano group in cyanocobalamin, or to the 5′ position of 5′-deoxyadenosine.

Those enzymes which bind adenosylcobalamin achieve their catalysis of group migrations by homolytic cleavage of the Co–C bond to form an adenosyl radical and cob(II)alamin. Enzymes which use methylcobalamin to catalyse methyl transfer reactions use heterolytic cleavage to yield cob(I)alamin and a methyl cation. Methionine synthase catalyses two successive methyl transfers (2.2) and (2.3):

$$CH_3{-}\text{cob(III)alamin} + \text{homocysteine} \Longrightarrow \text{cob(I)alamin} + \text{methionine}, \tag{2.2}$$

$$\text{cob(I)alamin} + \text{methyltetrahydrofolate} \Longrightarrow CH_3{-}\text{cob(III)alamin} + \text{tetrahydrofolate}. \tag{2.3}$$

The cobalamin prosthetic group comprises a cobalt atom ligated to four nitrogen atoms in the centre of a corrin ring, and a dimethylbenzimidazole nucleotide supplies an axial nitrogen ligand (see figure 4). Studies of analogue complexes have strongly suggested that it is the (lower) axial ligand which determines the bond strength and mode of cleavage of the Co–C bond (Halpern 1982).

Methionine synthase from *Escherichia coli* contains 1227 amino acid residues with molecular weight 136 kDa and has two functionally distinct regions. Methylcobalamin binding is in the NH_2-terminal, 98 kDa region and a 27 kDa, fragment containing the binding region was isolated by tryptic digestion and the structure determined at 3.0 Å resolution (Drennan *et al.* 1995). This study has provided the first evidence of the binding site of the methylcobalamin. There is a significant change in the coordination of the cobalt when methylcobalamin binds to the enzyme fragment. The

PHILOSOPHICAL TRANSACTIONS OF THE ROYAL SOCIETY A MATHEMATICAL, PHYSICAL & ENGINEERING SCIENCES

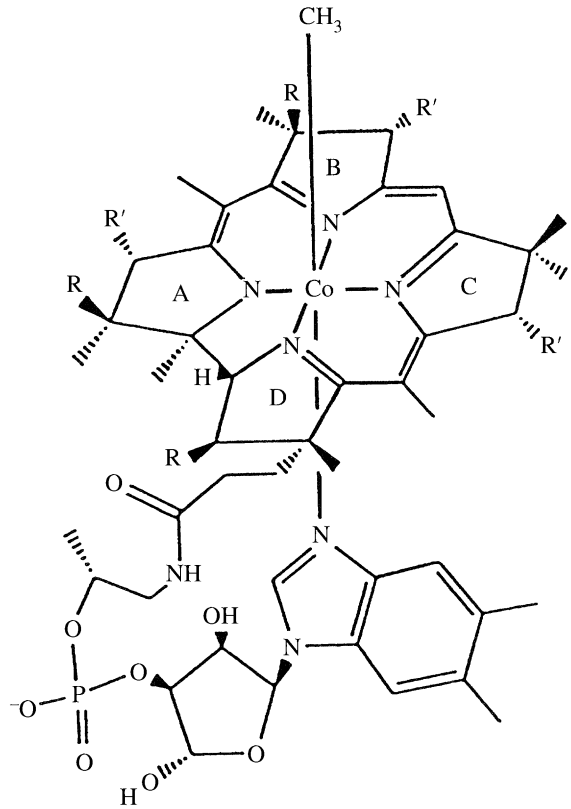

Figure 4. Representation of the structure of methylcobalamin (R = CH_2CONH_2; R' = CH_2 CH_2CONH_2); the nucleotide base dimethylbenzimidazole is connected to the D ring of the corrin by an unusual α sugar-nucleotide linkage and a ribose phosphorylated on the 3′, rather than the 5′, position (see Drennan *et al.* 1995).

dimethylbenzimidazole nucleotide no longer bonds to the cobalt, but is displaced and extended away from the corrin ring to form a 'nucleotide tail' bound inside a hydrophobic pocket. The imidazole ring of a histidine residue (His^{739}) from the enzyme fragment replaces the benzimidazole ligand in the lower axial position of the cobalt atom. The sequence Asp—X—His—X—X—Gly, which contains this histidine ligand, is conserved in several adenosylcobalamin-dependent enzymes, suggesting that the displacement of the dimethylbenzimidazole will be a feature common to many cobalamin-binding proteins. Thus, the cobalt ligand His^{759}, and the neighbouring residues Asp^{757} and Ser^{810}, may form a catalytic quartet, Co—His—Asp—Ser, that modulates the reactivity of the B_{12} prosthetic group in methionine synthase. Drennan *et al.* (1995) used EPR spectroscopy in conjunction with ^{14}N and ^{15}N labelling to study cob(II)alamin in the presence of methionine synthase in order to demonstrate that the crystal structure of the 27 kDa methylcobalamin-containing fragment of the enzyme was representative of the structural changes in the intact enzyme complex.

A second aspect of the structure is also unexpected. The upper face of the corrin, with the axially bound methyl group, is almost completely protected by hydrophobic residues from a helix bundle domain of the enzyme fragment. In the normal methylation cycle, the thiolate of homocysteine is proposed to attack the methyl group to produce methionine. However, in the bound form of the cofactor there is no room for

homocysteine to approach the methyl group. Thus, if this structure is representative of the situation in the intact enzyme:B_{12} complex then this information provides only the starting point for understanding the activity of the metal centre and the structural reorganization that may occur during catalysis (Stubbe 1995).

S-Adenosylmethionine is a third cofactor required for methionine biosynthesis and it is used to regenerate an active form of methionine synthase when the cob(I)alamin form requires regeneration from the cob(II)alamin, which appears to form occasionally on enzyme turnover in a non-catalytic reaction with, presumably, O_2. This means that all three accessible oxidation states of Co must be regulated in this enzyme, which surely provides a mechanistic link to the other class of cobalamin-dependent enzymes. The challenge is to understand how control of the chemistry of the Co—C bond is achieved.

(*e*) *Urease*

Urease, a nickel-containing enzyme, catalyzes the hydrolysis of urea, an abundant end product of metabolism, to form ammonia and carbonate. This enzyme degrades urea at *ca.* 10^{14} of the uncatalyzed rate and is vital for the supply of fixed nitrogen to bacteria, fungi, plants and some invertebrates. Urease was the first enzyme to be crystallized. This was accomplished some 70 years ago (Sumner 1926) for material isolated from jack beans and represented a vital advance, both scientifically and philosophically, since the crystallization provided proof that enzymes were well defined chemical compounds. Nickel was shown to be at the active site (Dixon *et al.* 1975) and it is now possible to discuss the role of this metal (Lippard 1995) following the determination of the structure of urease from *Klebsiella aerogenes* (Jabri *et al.* 1995).

Figure 5 shows the structure of the catalytic site of urease, which consists of two nickel atoms *ca.* 3.5 Å apart bridged by the carboxylate side chain of a special ligand. The ε-amino acid residue of Lys^{217} has reacted with CO_2 to produce a carbamate group. This feature explains why CO_2 is required for nickel-binding to metal-free urease (Park & Hausinger 1995). The coordination of each nickel is different (see figure 5): Ni(1) is bound to two N and one O atom (His^{246} through the Nδ atom, His^{272} through Nε, and a carbamate oxygen of Lys^{217}) Ni(2) is bound to two N and three O atoms (Nε of His^{134} and His^{136}, O of Asp^{360}, the second carbamate O of Lys^{217} and a water molecule). An uncertainty in the structure of the bimetallic site arises from the identification of some (weak) electron density which may allow Ni(1) to be decribed as pseudo-tetrahedral with a second water molecule, but not at full occupancy.

There is a striking resemblance between the amino acid arrangement for the bimetallic binding site of urease and that of the zinc enzyme adenosine deaminase which, however, only binds a single metal atom. A crucial difference is the modified Lys^{217} residue; the equivalent residue in adenosine deaminase is an aspartate (Asp^{181}), the side chain of which is too short to coordinate to the zinc. The longer polymethylene side chain of Lys^{217}, plus the carbamate group, clearly leads to binding to the metal and the stabilization of a bimetallic centre. This arrangement is clearly crucial to the function of the urease. The proposed mechanism (Dixon *et al.* 1980; Jabri *et al.* 1995; Lippard 1995) involves the coordination of urea ($(NH_2)_2CO$) by its oxygen to the three-coordinate Ni(2), leading to activation of the substrate by polarization. The H_2O molecule coordinated to Ni(1) is polarized and primed for conversion to OH^- which then attacks the carbon of the urea, leading to the formation of NH_3 plus $H_2NCO_2^-$ which, on protonation, forms NH_3 and CO_2.

PHILOSOPHICAL TRANSACTIONS OF THE ROYAL SOCIETY A MATHEMATICAL, PHYSICAL & ENGINEERING SCIENCES

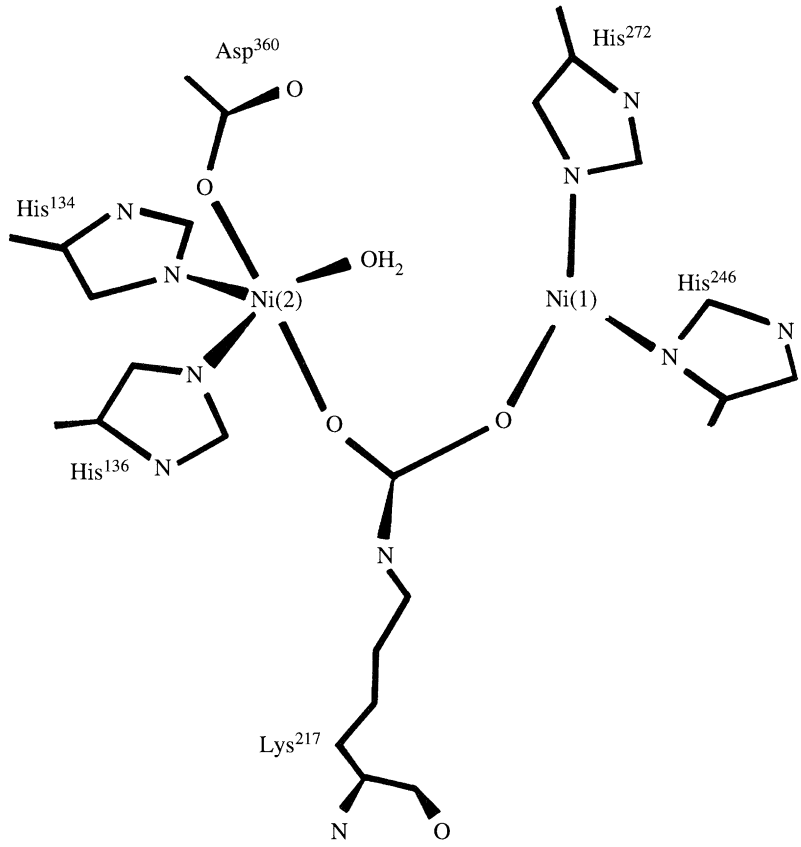

Figure 5. Representation of the structure of the catalytic site of urease (after Jabri *et al.* 1995).

(*f*) *Nickel–iron hydrogenase from Desulphovibrio gigas*

The standard redox couple comprising dihydrogen oxidation and proton reduction, $2H^+ + 2e^- = H_2$, is catalysed by three types of metal-containing enzymes in micro-organisms (Adams *et al.* 1990). The types are defined as Fe-hydrogenases, Fe–Ni H_2ases, and Fe–Ni–Se H_2ases. Proton reduction, leading to H_2 evolution, is part of pyuvate fermentation. H_2 oxidation is coupled to reduction of a variety of electron acceptors, such as O_2, NO_3^-, SO_4^{2-}, CO_2 and fumarate. The Ni–Fe H_2ase from *Desulphovibrio gigas* is a heterodimeric periplasmic protein comprising 60 kDa and 28 kDa subunits. One $[Fe_3S_4]$ and two $[Fe_4S_4]$ clusters are located in the 28 K subunit, which contains an amino-terminal domain, showing similarities to flavodoxin, a redox protein (Smith *et al.* 1977). The nickel atom is located in the 60 K subunit. EPR spectroscopy was used to identify the complexity of the reaction cycle of this enzyme. Two EPR signals for the aerobically isolated enzyme were associated with an 'unready' state (Ni–A) and a 'ready' state (Ni–B) (Cammack *et al.* 1987). The former state requires an activation time in the order of hours, whereas the latter state is rapidly reduced by H_2 to an 'active' form under anaerobic conditions. During this reduction, a photo-sensitive EPR signal, labelled Ni–C, develops and in the presence of light leads to another EPR signal, Ni–L (or Ni–C*). The rate of photolysis is much slower in D_2O than in H_2O (van der Zwaan *et al.* 1985). The one-electron reduction of Ni–B or Ni–C leads to EPR-silent states labelled Ni–SI and Ni–R (Barondeau *et*

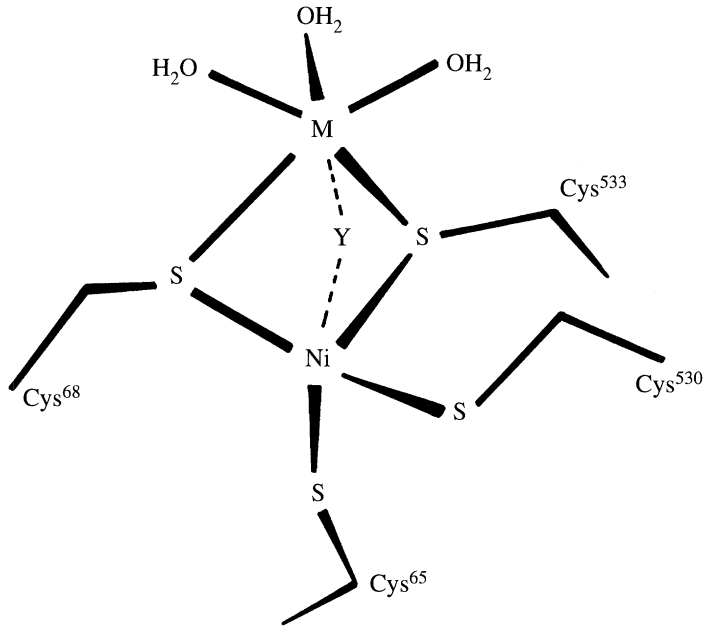

Figure 6. Representation of the bimetallic site of the nickel–iron hydrogenase from *Desulphovibrio gigas*; M is possibly Fe (see Volbeda *et al.* 1995).

al. 1994), respectively. Both EPR and Mössbauer spectroscopies have been used to monitor the redox levels of the Fe–S clusters. The midpoint redox potentials for the different nickel states correspond closely to those of the two $[Fe_4S_4]$ clusters (Teixeira *et al.* 1989). This contrasts with a relatively high midpoint redox potential for the $[Fe_4S_4]$ cluster, which appears to be absent from Ni–Fe–Se H_2ases.

The solution of the structure of the enzyme from *Desulphovibrio gigas* was obtained at 2.85 Å resolution by Volbeda *et al.* (1995). Interestingly, the smaller subunit is very similar in structure to the redox protein flavodoxin from *Clostridium MP* (Smith *et al.* 1977). The three Fe–S clusters in this smaller subunit, are almost linearly disposed, and the proximal and distal $[Fe_4S_4]$ clusters were defined on the basis of their distance from the Ni atom. The proximal cluster is conventionally bound by four cysteinyl sulphur atoms. However, this study has shown that the distal cluster has a novel set of cluster ligands comprising three cysteinyl sulphur atoms and one histidine residue, with the imidazole ring located on the surface of the protein. Three cysteinyl sulphur atoms bind the $[Fe_3S_4]$ cluster.

The coordination at the nickel atom is well defined by this study, in respect of four cysteinyl sulphur atoms: three 'equatorial' at *ca.* 2.25 Å and an 'apical' at *ca.* 2.60 Å (figure 6).

This structure determination appears to pose more questions than it answers about the active (nickel) site, since the site contains two metal atoms. The identity of the Ni atom is supported by the indirect evidence that it is a very weak anomalous scatterer of Cu—K_α radiation, whereas the second site gives a strong peak in an anomalous difference map. Additionally, in an Fe—Ni—Se H_2ase the selenocysteine homologous to one of the proposed cysteinyl ligands in the *Desulphovibrio gigas* enzyme has been shown, spectroscopically, to ligate nickel. Thus, of the four cysteinyl sulphur atoms, two are terminal to the nickel and two bridge between it and the second metal (M), which could be Co, Mn or V on the grounds of anomalous scattering,

but is considered to be iron. The active site model yields three water molecules as ligands to M, and possibly a third unidentified atom, labelled Y in figure 6, bridging Ni and M.

A crucial spectroscopic comparison was performed, which measured the EPR spectrum of crystals obtained under the same conditions as those used in the X-ray analysis. This spectrum indicated a mixture of *ca.* 85% Ni—A and *ca.* 15% Ni—B signals and that about only half the total Ni in the Ni—Fe H_2ase is EPR active. Further evidence from internal comparison of the two crystallographically independent H_2ase molecules strongly suggests considerable disorder in the active site. Thus, the overall disposition of the redox active centres in the two subunits has been defined, but the identity of the active site is still effectively unknown.

(*g*) *Methane monoxygenase*

Methanotrophic bacteria use methane as their source of carbon and energy and are important in the total carbon cycle since they consume the methane produced by anaerobic sediments and thereby limit the atmospheric concentrations of this 'greenhouse gas'. The reaction of methane with dioxygen produces methanol and water according to the following reaction:

$$CH_4 + NADH + H^+ + O_2 \rightarrow CH_3OH + NAD^+ + H_2O. \tag{2.4}$$

Methane monooxygenases (MMOs) of several of the bacteria consist of three proteins, which are a hydroxylase, a reductase and a coupling protein. MMOs will oxidize a broad range of hydrocarbon substrates (Colby *et al.* 1977; Liu *et al.* 1993) and indicate the potential uses of methanotrophic bacteria in decontamination and in fuel production. The hydroxylase enzyme, of formula weight 251 kDa is a dimer containing two diiron units, which are responsible for the methane oxidation (Lipscomb 1994; Rosenzweig & Lippard 1994). MMOs have been the subject of many detailed spectroscopic investigations of reaction intermediates (Lee *et al.* 1993; Liu & Lippard 1995). These results are now being combined with the information provided by crystallographic studies (Rosenzweig *et al.* 1995) of the hydroxylase component of soluble MMO from *Methylococcus capsulatus* (Bath); these have been accomplished at 2.2 Å resolution for crystals at 4 °C and at 1.7 Å resolution for crystals at −160 °C. The latter determination was performed for two different oxidation states of the enzyme.

In its oxidized form the enzyme (see figure 7) contains a diiron(III) centre with an Fe···Fe separation of 3.1 Å. Each iron is coordinated to the Nδ atoms of the imidazole ring of two non-contiguous histidine residues with Fe—N distances of *ca.* 2.1 Å, as determined for the structure at −160 °C and 1.7 Å resolution. There is a (semi-) bridging carboxylate from Glu^{144} with an Fe(2)—O bond length *ca.* 0.4 Å longer than a 'normal' bonding distance of *ca.* 2.0 Å. Fe(1) is further coordinated to a monodentate carboxylate oxygen atom from a Glu^{114} and Fe(2) is bound by two such carboxylate oxygen atoms (Glu^{209}, Glu^{243}). Fe(1) has a terminal water molecule as a ligand which is hydrogen bonded to the carbonyl carboxylate oxygen atoms of Glu^{114} and Glu^{243} on each iron atom. It should be noted that Glu^{243} is less well defined in the electron density maps than the other glutamate residues and may be disordered. Six coordination and approximately octahedral geometry at both iron atoms is completed by two bridging groups, which were revealed by difference Fourier electron density maps. These groups are assigned as μ_2—OH and μ_2—OH_2, the former bridge being asymmetric and located at *ca.* 0.3 Å closer to Fe(1) than to Fe(2); Fe(1)—OH 1.7 Å, Fe(2)—OH 2.0 Å. The bridging water molecule appears to

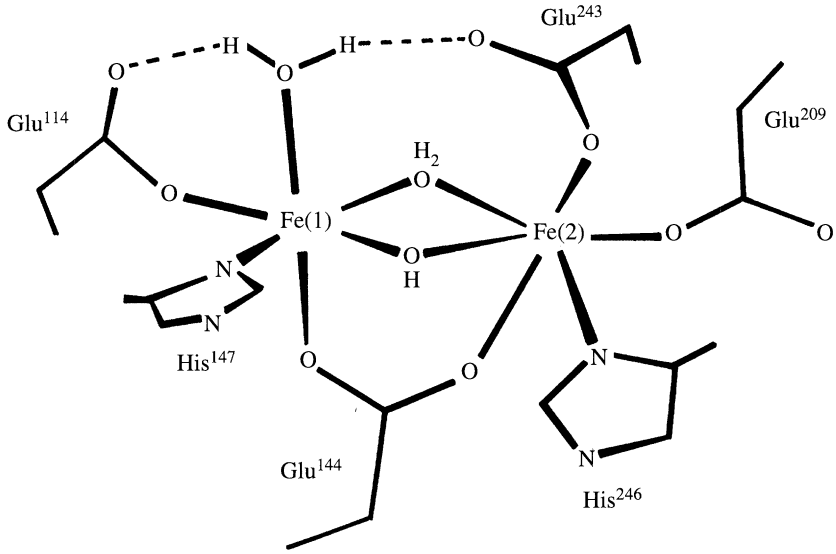

Figure 7. Representation of the structure of the dinuclear iron centre of methane monoxygenase from *Methylococcus capsulatus* (Bath) (see Rosenzweig *et al.* 1995).

be weakly coordinated at *ca.* 2.3 Å from Fe(1) and *ca.* 2.5 Å from Fe(2). The dimeric nature of this enzyme means that there are two crystallographically independent diiron centres present. The estimated standard deviation in bond distances at the diiron site was *ca.* 0.2 Å, which means that one must be cautious when identifying significant differences between the metal sites; thus, the asymmetric nature of the bridging arrangement within the iron dimers is not outside the experimental error.

This structure has important differences from an earlier study of the same enzyme (Rosenzweig *et al.* 1993) which was performed at 4 °C and to 2.2 Å resolution. The bridging water molecule (figure 7) was replaced by a bridging acetate, presumably derived from the NH_4OAc in the crystallisation buffer, and there was a concomitant increase in the Fe(1) $\cdots$ Fe(2) distance from 3.1 Å to 3.4 Å. The Fe $\cdots$ Fe distance in this and other diiron enzymes is a source of much debate. In principle, EXAFS might be expected to afford a good measure of the Fe $\cdots$ Fe distance. However, the distance of interest is at the upper limit of reliability for the technique, especially as a large number of backscattering contributions arise at this distance from outer shells of ligands.

A potential problem also arises in the use of synchrotron radiation to obtain EXAFS spectra and X-ray diffraction data are collected with that source. Thus, during EXAFS data collection, many oxidized MMO samples from *Methylococcus capsulatus* were photoreduced to a mixed-valent (Fe^{III}, Fe^{II}) state by the intense synchrotron X-ray beam (DeWitt *et al.* 1995). However, Rosenzweig *et al.* (1995) have considered this problem and deduced that no photoreduction occurred during crystallographic data collection because: (i) the refined structure of the diiron moiety showed no trends in bond lengths which could be ascribed to distinct Fe^{II} and Fe^{III} sites; and (ii) a control experiment in which EXAFS spectra were collected on single-crystal samples of oxidized MMO showed no shift in the Fe *K*-edge position, which would have been expected if photoreduction had occurred.

Crystals of oxidized MMO from *Methylococcus capsulatus* (Bath) were chemically reduced by soaking in a solution containing sodium dithionite and methyl viologen.

The diffraction data were again collected at −160 °C and solved to 1.7 Å resolution. The structure was very similar to that of the oxidized MMO (figure 7), except for one of the diiron centres (protomer A). Each iron atom is coordinated by one Nδ of a histidine ligand and the semi-bridging glutamate (Glu^{144}) carboxylate is still present. There is also one terminal glutamate (Glu^{114} and Glu^{209}) carboxylate oxygen atom on each iron atom. However, Glu^{243}, which was found as a monodentate terminal ligand to Fe(2) in oxidized MMO (and also has this bonding mode in protomer B of the reduced enzyme), has become a bidentate chelate to Fe(2) and, additionally, one oxygen atom bridges to Fe(1). This glutamate residue is the least well-defined in terms of electron density, as was also found in the oxidized form of the enzyme. Within protomer A of the reduced enzyme, the terminal water molecule bound to Fe(1) and the bridging water molecule, more distant from Fe(2) than Fe(1), remain present after reduction, but there is no evidence for a bridging hydroxide. Spectroscopic studies (DeRose *et al.* 1993) have shown that the fully oxidized (Fe^{III}, Fe^{III}) and mixed-valent (Fe^{III}, Fe^{II}) forms of MMO each contain a μ_2—OH bridge. Therefore, protomer A in the reduced crystals was assigned to a fully reduced (Fe^{II}, Fe^{II}) state and involves an Fe···Fe separation of 3.28 Å. The only significant difference between the diiron sites of protomer B in the reduced enzyme and those of the oxidized centres of MMO's (figure 7) is the Fe···Fe distance of 3.43 Å, as compared to 3.1 Å.

The change in the coordination mode of Glu^{243} between oxidized and reduced forms of the MMO form *Methylococcus capsulatus* (Bath) is illustrative of a 'carboxylate shift' (Rardin *et al.* 1991). These studies all point to a considerable flexibility within the active site of MMOs, which suggests possibilities for the control of activity and processing of substrates and products.

(*h*) *Purple acid phosphatase*

Purple acid phosphatases (PAPs) catalyse the hydrolysis of activated phosphoric acid esters like adenosine triphosphate in the pH range 4 to 7 (Vincent *et al.* 1991). In mammalian enzymes, the dinuclear metal site comprises an antiferromagnetically coupled Fe^{III}—Fe^{II} centre, whereas the kidney bean (KB) enzyme has a Fe^{III}—Zn^{II} dinuclear centre. KBPAP is a homodimeric protein of 111 kDa mass, containing 432 amino acid residues per monomer, and the structure has been determined at 2.9 Å resolution (Sträter *et al.* 1995). Each monomer consists of two domains and the two dinuclear centres are 35 Å apart. The iron (see figure 8) is coordinated by a tyrosine (Tyr^{167}) phenolate oxygen atom, which is responsible for the characteristic purple colour resulting from the tyrosine-metal charge transfer transitions at 560 nm.

Iron is also ligated by an imidazole nitrogen atom from His^{325} and a monodentate carboxylate from Asp^{135}. The zinc is ligated by two imidazole nitrogen atoms from His^{286} and His^{323} and the amide (carbonyl) atom of an Asn^{201}. The two metals are bridged by a monodentate carboxylate oxygen atom from Asp^{166}. The electron density map at this resolution does not reveal any unambiguous indication for additional ligands, but the model used to refine the dinuclear site included a terminal hydroxy ligand to iron, a terminal aqua ligand to zinc, and a —OH bridge between the two metals. In this model the geometry of the iron site is almost perfectly octahedral, whereas the zinc site is distorted.

Proposals for the solvent molecules/ions drew on the results of the postulated reaction pathway and spectroscopic studies. Interestingly, KBPAP shows almost identical spectroscopic and kinetic behaviour after exchange of Zn^{II} by Fe^{II} (Suerbaum *et al.*

PHILOSOPHICAL TRANSACTIONS OF THE ROYAL SOCIETY A MATHEMATICAL, PHYSICAL & ENGINEERING SCIENCES

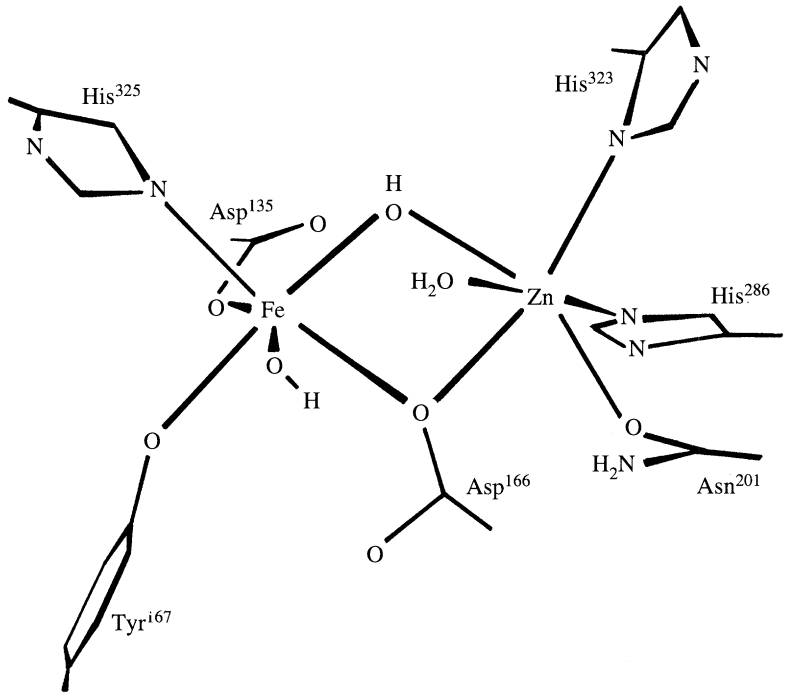

Figure 8. Representation of the iron–zinc centre of kidney bean purple acid phosphatase (see Sträter *et al.* 1995).

1993, 1995); however, the absorption maximum of the Fe_2^{III} KBPAP does not shift from 560 to 515 nm on reduction, as seen for the mammalian enzymes. The Fe^{III}—Zn^{II} distance in KBPAP is 3.1 Å, but EXAFS measurements on frozen solutions (Priggermeyer *et al.* 1995) give a metal–metal distance of 3.9 Å. This significant discrepancy needs to be resolved.

The location of the active site of KBPAP is at the carboxy end of two sandwiched β sheets, whereas other diiron proteins, such as hemerythrin (Holmes *et al.* 1991), ribonucleolide reductase (Nordlund *et al.* 1990) and methane monooxygenase (Rosenzweig *et al.* 1993, 1995) have the dimeric metal fragment bound between the α helices of a four-helix bundle. For further comparison, the Zn $\cdots$ Zn distance in the trinuclear Zn_2Mg enzyme alkaline phosphatase (Kim & Wyckoff 1991) is 3.9 Å. Therefore, it has been suggested that the mechanism of phosphate ester hydrolysis proceeds in the same way for the two enzymes, but that the weaker Lewis acidity of Zn^{II} compared to Fe^{III} results in a shift in the response of the reaction to changes in pH. Thus, the protein structure determination has been successful in allowing gross structural comparisons and providing important details of the active (metal) site.

(*i*) *Human ceruloplasmin*

Human ceruloplasmin (hCP) is a copper-containing glycoprotein of molecular weight *ca.* 132 kDa, comprising a single polypeptide chain of 1046 amino acid residues and between 7 and 8% carbohydrate content (Takahashi *et al.* 1984). hCP is classified as a multinuclear blue copper oxidase which, on isolation and purification, is very susceptible to proteolytic cleavage, aggregation and loss of copper. Ceruloplasmins are multifunctional plasma proteins and have been associated with copper transport,

ferroxidase activity (Dancis *et al.* 1994), amine oxidase activity and antioxidant activity. However, the precise biological functions of hCP have not yet been elucidated.

The X-ray structure of hCP has been determined at 3.1 Å resolution (Zaitseva *et al.* 1996) and shows that the molecule contains six copper atoms and is arranged in six domains. Domains 2, 4 and 6 each contain a single copper atom and a trinuclear copper array spans domains 1 and 6. The mononuclear Cu atoms in domains 4 and 6 are bound by two histidine N atoms, a cysteine S and a methionine S, which is typical of a type-I copper centre. Also, a carbonyl oxygen atom from a leucine residue may be within bonding distance of the copper atom, as has been found in the oxidized form of azurin from *Alcaligenes denitrificans* (Baker 1988; Nar *et al.* 1991). The mononuclear copper centre in domain 2 lacks the methionine residue and this is replaced by a leucine residue, although not oriented to function as a ligand. The three copper atoms form an approximate equilateral triangle of side *ca.* 18 Å.

The triangular copper cluster lies outside the triangle of the three mononuclear copper centres and *ca.* 12–13 Å from the mononuclear copper site of domain 6. Two of the three copper atoms are designated as a type-III site and are each bound by three histidine N atoms. The model for the electron density in this domain includes an oxygen atom bridging the two metals. The third copper atom, more distant from the mononuclear site in domain 6, is bound by two histidine N atoms and a further oxygen atom. This model for the binuclear site is consistent with that found previously for ascorbate oxidase (AO) (Messerschmidt *et al.* 1992). Indeed, a striking overall organizational similarity has been detected between the configurations of domains 1, 2 and 3 of AO and domains 1, 2 and 6 of hCP. Similar comparisons with the copper enzyme nitrite reductase (Godden *et al.* 1991) reveals comparable spacial arrangements of domains and implies a common ancestral protein for all three copper-containing molecules.

Thus this study has been very successful in revealing the organization of hCP and identifying the likely ligands to the copper centres. However, the limitation imposed by the resolution in the study means that the details of the coordination geometry at the metal sites remain undefined.

3. X-ray absorption spectroscopy

(*a*) *Introduction*

Since the first experiment on an intense synchrotron radiation source (Kincaid & Eisenberger 1975), X-ray absorption spectroscopy (XAS) has become established as a technique for investigating the local environment of metal atoms in proteins. XAS has many advantages as a probe of metal centres in biological systems and numerous studies have been reported in the literature (Cramer & Hodgson 1979; Powers 1982; Scott 1985; Garner 1991). The X-ray absorption spectrum of Cu_5Zn_3-metallothionein (figure 9) shows the element specificity of the technique and regions within the profile of an absorption edge. Beyond the absence of a requirement for crystalline material, major attractions encouraging the application of XAS include the specificity and sensitivity of the technique, so that information can be obtained for a particular metal centre presented at (say) one atom in 10^6 in a large and complicated protein. Also, XAS allows several different states of a system to be probed with relative ease—thereby providing a profile of how a metal centre responds, for example, to the oxidation level of an enzyme, the presence of substrates, substrate analogues or inhibitors.

PHILOSOPHICAL TRANSACTIONS OF THE ROYAL SOCIETY A MATHEMATICAL, PHYSICAL & ENGINEERING SCIENCES

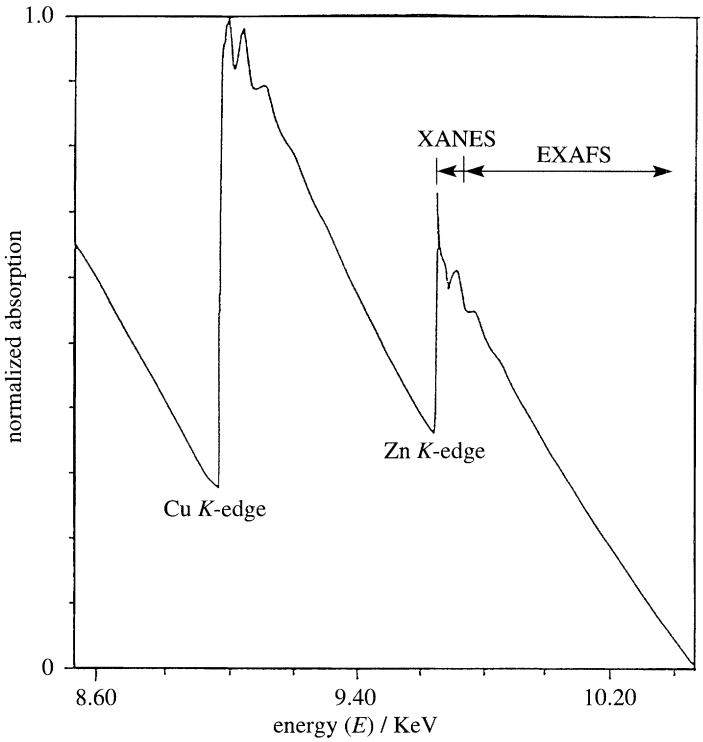

Figure 9. X-ray absorption spectrum of Cu_5Zn_3-metallothionein.

(*b*) *Information content of XAS*

The actual energy of a particular X-ray absorption edge of an element depends upon the oxidation state and the nature of the immediate chemical environment of that element. Typically, one unit increase of oxidation state increases the 3d or the 4d element edge position by 1–3 eV. Labhardt & Yuen (1979) observed a shift in the position of the iron *K*-edge and its associated structure of *ca.* 1.5 eV to higher energy upon oxidation of cytochrome c. The sense and magnitude of this shift are consistent with a redox process which is concentrated at the iron centre. Excitation of a core electron into the continuum may be convoluted with transitions to the valence levels. These promotions give rise to pre-edge and edge features which can provide information concerning the chemical nature and electronic structure of the primary absorber.

Beyond the X-ray absorption edge, oscillations in the amplitude of the absorption can extend for up to 1000 eV. Historically, and more recently because of the different theoretical treatment necessary to interpret the data, it has been customary to classify the oscillations within *ca.* 50 eV of the edge as the X-ray absorption near edge structure (XANES) and those which extend beyond this region as the extended X-ray absorption fine structure (EXAFS). The theoretical basis of the latter is considered mature and interpretations of EXAFS data have been reported confidently for over a decade. In contrast, progress in the understanding and, therefore, the application of XANES has been relatively slow and data in this spectral region are generally not interpreted but used qualitatively to 'fingerprint' a metal site. EXAFS provides structural information concerning the distance, nature, number and coherence of the shells of atoms around the primary absorber. Phase shifts for analysis of EXAFS can

now be considered reliable, whether extracted from chemical systems or calculated *ab initio*. However, confidence in the interpretation of the EXAFS of a metalloprotein centre is significantly increased by the successful completion of the corresponding exercise for a related and structurally characterized chemical analogue.

The primary sources of uncertainty in the structural parameters determined from EXAFS analysis arise from the correlation between the coordination number (N) and the Debye–Waller factor (σ^2) of individual shells of backscatterers. The usual accuracy which can be expected for the primary coordination shell of a metal centre in a protein is $R \pm 0.03$ Å, $N \pm 25\%$ and $Z \pm 1$. The present limitations in defining N and Z are especially frustrating and emphasize the need to integrate the information available from other spectroscopic and structural techniques into EXAFS analyses. Amino acid sequence data and/or site-directed mutagenesis studies can provide clear indications of the nature of the groups binding metals in metalloproteins. Futhermore, as illustrated by studies on rubredoxin (Shulman *et al.* 1978) and Cu, Zn-superoxide dismustase (Blackburn *et al.* 1984), XAS and protein crystallography are especially complementary.

When contemplating the use of XAS in general, and EXAFS in particular, to probe a metal centre within a protein or when considering the results of such studies, the following should be noted:

(i) angular information is not obtained unless oriented samples are investigated;

(ii) rarely does the structural information extend beyond 4 Å from the primary absorber;

(iii) the spectrum sums data for all atoms of a particular element and, if the element of interest is present in more than one chemical form, an average environment is obtained;

(iv) the possibility of radiation damage must be anticipated and the integrity of samples should be monitored after, and if possible during, measurement.

(*c*) *Molybdenum and vanadium nitrogenases*

One of the earliest applications of EXAFS to probe a metalloenzyme was the study of the molybdenum site of nitrogenase in the *Clostridium pasteurianum* and *Azotobacter vinelandii* MoFe-proteins and the isolated iron–molybdenum cofactor (FeMoco) (Cramer *et al.* 1978*a*, *b*; Conradson *et al.* 1987; Liu *et al.* 1994). These studies showed definitively that molybdenum is present as part of a polynuclear cluster containing sulphur and iron, with Mo–S and Mo–Fe distances of 2.35 and 2.72 Å, respectively. This work inspired the successful development of many chemical systems containing Mo–Fe–S clusters and XAS studies of these systems strengthened the interpretation of corresponding data for the natural system. The environment proposed is compatible with the results of protein crystallographic investigations (Kim & Rees 1992; Chan *et al.* 1993; Bolin *et al.* 1993). Thus, the molybdenum is located at one end of an $MoFe_7S_9$ cluster, ligated to three sulphurs of this framework, the imidazole group of His^{442} and two oxygens from homocitrate. The Mo K-edge EXAFS data provide accurate interatomic distances for the molybdenum environment in isolated FeMoco as: three O/N atoms at 2.19 Å, three sulphur atoms 2.37 Å and three iron atoms at 2.70 Å, with similar values being obtained for the MoFe-protein (Liu *et al.* 1994). These results identified a Mo$\cdots$Fe separation of 5.1 Å, corresponding to the three equivalent iron atoms in the other 'half' of the cluster. Thus, the Mo K-edge and Fe K-edge (Arber *et al.* 1988) EXAFS information combine with the protein crystallographic information to give a clear view of the structure of FeMoco in the resting reduced state of the MoFe-protein.

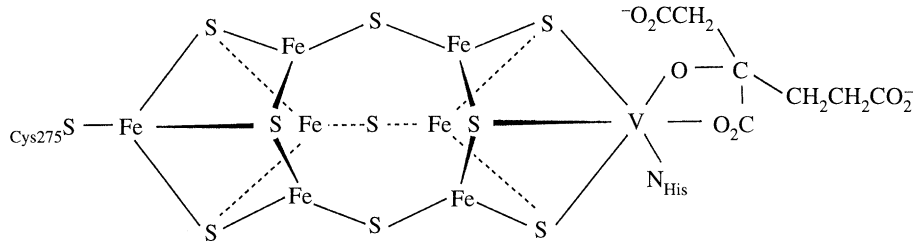

Figure 10. Proposed structure of the iron–vanadium cofactor (FeVaco) of the vanadium nitrogenase enzymes based on the structure of its molybdenum counterpart (Kim & Rees 1992; Chan *et al.* 1993; Bolin *et al.* 1993) and vanadium *K*-edge XAS studies (Arber *et al.* 1987; George *et al.* 1988).

Genetic suppression of the 'normal', molybdenum-dependent nitrogenase of certain classes of *Azotobacter* allows expression of the vanadium-dependent enzyme. The vanadium and molybdenum nitrogenase systems show many similarities and an iron–vanadium cofactor (FeVaco), analogous to FeMoco, has been isolated (Eady 1995). Clear evidence of a strong similarity between active sites in the MoFe- and VFe-proteins has been provided by vanadium *K*-edge XAS studies but, so far, no crystallographic studies have been reported for the VFe-protein. VFe-proteins from *Azotobacter chroococcum* (Arber *et al.* 1987) and *Azotobacter vinelandii* (George *et al.* 1988) have been investigated by XAS. The edge structure shows a weak single 1s–3d transition, the intensity of which precludes the presence of terminal V = O bonds and implies an octahedral coordination around vanadium. The edge and XANES structure is very similar to that recorded for vanadium in the cubane-like cluster of $[NMe_4][VFe_3S_4Cl_3(DMF)_3]$ and the EXAFS results are consistent with vanadium in the VFe-protein of *Azotobacter chroococcum* being in an environment of three oxygen (or nitrogen), three sulphur and three iron atoms at distances of *ca.* 2.13, 2.33 and 2.75 Å, respectively.

The average environment of iron in FeMoco (Arber *et al.* 1988) and FeVaco (Harvey *et al.* 1990) has been investigated by XAS. The results show that the two cofactors possess the same molecular topology, especially as the Fe···Fe distances across the central portion of the structure (figure 10) at 3.6–3.7 Å are clearly manifest in the EXAFS. *Vanadium would thus appear to substitute directly for molybdenum in FeMoco to form FeVaco* (see figure 10). The role of molybdenum and vanadium in the catalysis of N_2 reduction remains to be elucidated. Possibly they facilitate electron transfer to and/or redox reactions within the cluster. Therefore, it is noteworthy that XAS studies indicate that neither the molybdenum nor the vanadium centre experiences any significant structural change as the oxidation level of the cofactor is varied.

(*d*) *Oxomolybdoenzymes and their tungsten relatives*

XAS has played a vital role in defining the chemical nature of molybdenum centres in the oxomolybdoenzymes and how they respond to changes in the oxidation level of the molybdenum cofactor (Moco—see § 2 *c*) and/or to the presence of substrates, substrate analogues or inhibitors of enzymic activity (Hedman *et al.* 1990). Mo=O groups give rise to a low-energy edge-inflection due to a transition from the *K* shell to the Mo=O π^* orbital. This has been a ubiquitous feature of the molybdenum *K*-edge XAS studies of the oxomolybdoenzymes, as opposed to the nitrogenases.

The molybdenum *K*-edge EXAFS results achieved (George *et al.* 1989) for chicken liver sulphite oxidase are the clearest such data and the interpretation achieved rep-

resents a prototype for other oxomolybdoenzymes. The molybdenum site has been investigated in each of its three accessible oxidation levels ((VI), (V), and (IV)) as a function of pH and chloride concentration. The molybdenum(VI) is coordinated by two oxo-groups, at *ca.* 1.70 Å, one oxygen (or nitrogen) and three sulphur-donor ligands at *ca.* 2.06 and 2.42 Å, respectively; two of these sulphur atoms are presumably derived from the molybdopterin (see figure 3). The molybdenum(V) and (IV) centres each possess a single oxo-ligand, at *ca.* 1.69 Å, one oxygen (or nitrogen) and three sulphur-donor ligands at *ca.* 2.00 and 2.37 Å, respectively. Both of these centres appear to bind chloride at pH 6 in 0.3M KCl. EPR spectroscopy showed that the centre can exist in two different forms, which are in a pH- and anion-dependent equilibrium. The molybdenum *K*-edge EXAFS data are consistent with one chloride ligand binding to the low pH form and with the number of oxo-groups remaining the same in the high- and low-pH molybdenum(V) forms. Thus, reduction of molybdenum(VI) results in the loss of one oxo-group, presumably due to protonation, and the generation of an anion binding site. This behaviour is consistent with the chemistry of molybdenum in its higher oxidation states, since a *cis*-$\{Mo^{VI}O_2\}^{2+}$ centre is generally converted into a $\{Mo^{V}O\}^{3+}$ or $\{Mo^{IV}O\}^{2+}$ centre upon reduction and sites *trans* to an oxo-group are generally labile.

Xanthine oxidase is the most accessible of the oxomolybdoenzymes and is readily extracted from cows' milk. This enzyme exists in two forms: an active and an inactive form caused by loss of a sulphur atom (desulpho). Molybdenum *K*-edge EXAFS studies (Turner *et al.* 1989) have shown that the environments of molybdenum(VI) and molybdenum(IV) in desulpho xanthine oxidase closely resemble that of the corresponding oxidation state for chicken liver sulphite oxidase *vide supra.* The principal difference between the centre of the oxidized active form, as compared to oxidized desulpho form, is the presence of one sulphido-group (at *ca.* 2.18 Å) plus one oxo-group, rather than two oxo-groups. The molybdenum centre of xanthine oxidase is very reactive and both molybdenum *K*-edge EXAFS and EPR data indicate that the centre of this reactivity is the Mo=S bond. The terminal sulphido-group is lost upon reduction, presumably being protonated to form an Mo—SH moiety. Arsenite is a potent inhibitor of xanthine oxidase clear evidence for an Mo—S—As interaction, and an interbond angle of *ca.* 80° has been obtained from combined Mo and As *K*-edge EXAFS studies (Cramer & Hille 1985).

(*e*) *Ferritins*

Iron can be said to be the most chemically versatile of all the elements used by nature. It is essential for dioxygen uptake and transport in the vast majority of living systems, ubiquitous in electron transfer relays and oxygen metabolism, used widely as the catalytic centre in a large number of enzymes, and vital for DNA synthesis. However, the problem with storing large quantities of free iron in the body under physiological conditions is that soluble iron(III) reacts to form insoluble iron(III) oxide, the accumulation of which is toxic to cells. To avoid this, evolution has produced two iron storage proteins: ferritin and haemosiderin.

The major iron storage protein, ferritin, has been extensively studied (Ford *et al.* 1984) and shown to consist of a hollow spherical proteinaceous shell surrounding an iron(III) oxide–hydroxide core. Assuming that the cavity of ferritin is filled by an iron oxyhydroxide aggregate with a density of 2 g cm^{-3}, up to 4500 irons could be accommodated, but experimentally the maximum loading is *ca.* 2500 iron atoms. This suggests that there is an element of random distribution in operation, possibly

because of disorder and inefficient packing of the cavity. Furthermore, it is not known whether the iron centres in ferritin form one crystallite or several smaller crystallites. Thus, the ferritin core contains encapsulated portions of a crystal lattice (or lattices) which are too small to be treated as infinite arrays: a necessary assumption in the interpretation of X-ray diffraction patterns. Therefore, the detailed molecular structure of the ferritin core has been hard to discover and XAS has, so far, provided the only structural information.

Iron *K*-edge XAS studies have been accomplished for ferritin (Islam *et al.* 1989; Mackle *et al.* 1991) and haemosiderin (Mackle *et al.* 1991). These have allowed a direct comparison of structural aspects of the iron-oxide cores of ferritin and haemosiderin, which could only be inferred from other techniques. The EXAFS recorded for horse-spleen ferritin and 'normal' haemosiderin are indistinguishable, consistent with them possessing an identical iron-oxyhydroxide core. The data are indicative of an average environment of the iron(III) consisting of six oxygen atoms at *ca.* 1.96 Å and a split shell of iron atoms at *ca.* 3.01 and 3.43 Å, together with a further oxygen shell at *ca.* 3.54 Å (Heath *et al.* 1996). These Fe···Fe distances provide a clear indication of the nature of the iron hydroxide assembly and clusters such as $[Fe_{17}(\mu_3 - O)_4(\mu_3 - OH)_6(\mu_2 - OH)_{10}(heidi)_8(H_2O)_{12}]^{3+}$ ($H_3heidi = N(CH_2CO_2H)_2(CH_2CH_2OH)$) (Powell *et al.* 1995) are more appropriate than infinite lattices as structural models for the core of ferritin (Heath *et al.* 1996).

The nanoscale synthesis of inorganic particles is currently of great interest in materials chemistry. One possible route to the preparation of such materials involves the use of preorganized biomolecular architectures as chemically and spatially confined environments for the construction of inorganic clusters and nanoparticles. The polypeptide cage of ferritin has been used to prepare nanocomposites (Meldrum *et al.* 1991). An advantage of this biomimetic approach is that the inorganic nanoscale materials can be rendered biocompatible by virture of their intimate association with the surrounding polypeptide assembly. Thus, if appropriate synthetic routes could be developed, bioinorganic nanoparticles might be useful as biological sensors and markers, drug carriers, and diagnostic and bioactive agents. Nanocomposites housed within the ferritin shell include an Fe—S system and MnOOH; the metal environments of both have been probed by XAS. For the former, amorphous iron sulphide minerals containing either 500 or 3000 iron atoms have been synthesized *in situ*. ^{57}Fe Mössbauer spectroscopy indicates that most of the iron atoms in the 3000 iron atom cores are as Fe(III), whereas in the 500 iron atom clusters, approximately 50% of the iron atoms are Fe(III) with the remaining atoms having an effective oxidation state of about +2.5. Iron *K*-edge EXAFS for the 500 iron atom nanocomposite are consistent with a disordered array of edge-shared FeS_4 tetrahedra, connected by $Fe(S)_2Fe$ bridges with bond lengths similar to those of the cubane-type motif of iron–sulphur clusters (Douglas *et al.* 1995). For Mn in ferritin, the Mn *K*-edge position indicates that ferritin stabilizes Mn(III) and the interpretation of the EXAFS reveals that the (average) local environment of the metal has an inner coordination sphere of six oxygens showing the Jahn–Teller distortion generally associated with Mn(III): four oxygens at 1.91 Å, one at 2.14 Å, and one at 2.31 Å. The Mn···Mn separations of 2.88 Å are typical of edge sharing of the $Mn^{III}O_6$ moieties linked by μ-oxide and/or μ-hydroxide groups; the Mn···Mn separations of 3.10 and 3.94 Å are attributed to vertex sharing of the $Mn^{III}O_6$ centres (Mackle *et al.* 1993).

PHILOSOPHICAL TRANSACTIONS OF THE ROYAL SOCIETY A MATHEMATICAL, PHYSICAL & ENGINEERING SCIENCES

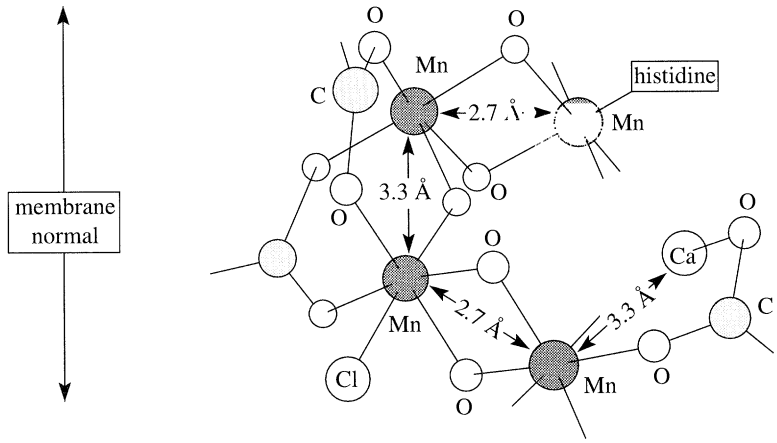

Figure 11. Structure of the Mn_4 centre of photosystem II based on Mn K-edge EXAFS studies of *Synechococcus* (Yachandra *et al.* 1993).

(*f*) *The manganese centre of photosystem II*

The photosynthetic water-splitting enzyme of chloroplasts is the source of dioxygen on this planet. The enzyme is located in the thylakoid membrane and, during turnover, it donates electrons to photosystem II and then oxidizes two molecules of H_2O to produce one molecule of O_2. Analytical and spectroscopic studies have demonstrated that a polynuclear manganese cluster is present at the heart of this enzyme and current interpretations favour the presence of an Mn_4 centre. Manganese K-edge XAS studies of photosystem II, combined with EPR data, have been influential in discussions of the oxidation state of the Mn_4 centre at various stages in the photolysis cycle, which oxidizes the reaction centre from S_0 to S_4 in four one-electron steps, prior to the release of O_2 and the reformation of S_0.

The position of the inflection point of the Mn K-edge and the shape of the edge provide information concerning the average oxidation state of the Mn_4 centre and its environment. Studies of photosystem II from *Synechococcus* (Yachandra *et al.* 1993) favour $\{Mn(III)\}_2\{Mn(IV)\}_2$ for the oxidation level of the S_1 state. The XANES profile is indicative of an environment of O and N atoms around the Mn atoms; this is augmented by the EXAFS which leads to the proposed model for the Mn_4 centre shown in figure 11. The (average) Mn–O/N environment consists of about two atoms at 1.82 Å and a total of 2–4 atoms at the distances of 1.95 and 2.15 Å. The location of Ca^{2+} is suggested by the change in the EXAFS and its Fourier transform upon depletion of Ca^{2+} and reconstitution by Sr^{2+}. These and other Mn K-edge EXAFS studies of photosystem II show that for the transitions $S_1 \rightarrow S_2$ and $S_2 \rightarrow S_3$ the structure of the manganese cluster changes only slightly; thus, no substantial structural reorganization of the Mn_4 centre occurs during the accumulation of these oxidizing equivalents. Chloride is a crucial cofactor which is necessary for the oxidation of the Mn_4 centre after the S_1 state. XANES spectra at the Mn K-edge indicate that the lack of chloride does not cause a gross structural modification of the cluster (Ono *et al.* 1995), a conclusion not incompatible with the structure in figure 11.

The Mn$\cdots$Mn separations are an important aspect of the Mn_4 centre. The 2.7 Å separation is consistent with the presence of μ_2-oxide or hydroxide groups, as in Mn-reconstituted ferritin (see § 3 *e*), and the 3.3 Å separation would be compatible with the proposed μ_2-carboxylate ligation. The dichroism observed for the Mn$\cdots$Mn

PHILOSOPHICAL TRANSACTIONS OF THE ROYAL SOCIETY A MATHEMATICAL, PHYSICAL & ENGINEERING SCIENCES

vectors for different orientations of the sample are consistent with an alignment of the 2.7 Å vectors approximately parallel to the plane of the membrane. Many challenges remain in the definition of the reaction centre of photosystem II and how the oxidation and coupling of two H_2O molecules is achieved. However, XAS has provided valuable information including the first indications of the structure of the Mn_4 centre.

4. Bond valence sum analysis (BVSA)

(*a*) *Introduction*

The concept of a 'bond' does not occur directly in either quantum mechanics or in ionic models, but is a term readily used in the description of all chemical structures and, by extension, biological molecules. The bond valence sum evolved from the efforts to formalize the 'properties' of the chemical bond. Pauling (1929) initiated the process when he introduced the idea of the bond strength of a bond in one of his 'principles determining the structure of complex ionic crystals'. He reasoned that the electric charge of each cation must balance the strength of the electrostatic valence bonds reaching it from the surrounding anions. Thus, for each cation, equation (4.1) applies where V_i is the valence (the formal oxidation state) of the cation, N_i is the coordination number of the cation, and s_{ij} is often referred to as the 'Pauling bond strength':

$$s_{ij} = V_i/N_i. \tag{4.1}$$

Brown & Altermatt (1985) proposed the use of equation (4.2), based upon Pauling's electrostatic valence principle, to describe the relationship between bond valence and bond length:

$$s_{ij} = \exp((r_0 - r_{ij})/B), \tag{4.2}$$

where s_{ij} is the bond valence of the bond r_{ij} between cation i and anion j and r_0 is a constant calculated for a particular cation–anion pair and is defined as the length of a bond of unit valence. The bond valence sum parameters r_0 and B were refined (Brown & Altermatt 1985) using bond length data contained in the inorganic crystal structure database (Bergerhoff *et al.* 1983) and the parameters were calculated by fitting equation (4.3), relating the oxidation state of the cation to the sum of the contributions from each bond between the cation and the ligands to the actual oxidation state of the metal centre:

$$V_i = \sum_j s_{ij}. \tag{4.3}$$

From the analysis of the variation of r_0 with the position of the ions in the Periodic Table, Brown & Altermatt (1985) proposed equation (4.4) for the calculation of r_0 values for cation–anion pairs for which data are not available; r_c and r_a are contributions to r_0 from the cation and anion, respectively:

$$r_0 = r_c + Ar_a + P - D - F. \tag{4.4}$$

A has a value of 0.8 for transition metals, otherwise it has a value of 1.0, and P, D and F are corrections required when the cation contains non-bonding p, d, and f electrons, respectively. The values of P and F are given by $P = 0.0175 \times$ (cation period $- 2$) and $F = 0.016 \times$ number of f electrons and the values of D are tabulated by Brown & Altermatt (1985). Equation (4.4) can reproduce the refined values of r_0 to within

0.013 Å and may give more reliable values of r_0 for bond length data sets containing a small number of metal centres. The values of r_0 for over 100 cation–anion pairs refined from over 600 environments were presented. The BVSA approach is widely used by geologists to calculate the oxidation state of metal centres in minerals or to determine the valency of bonds.

Pidcock *et al.* (1993) have investigated an alternative application of the correlations provided by BVSA. If reasonably reliable values of r_0 can be obtained from structural data available for coordination complexes contained within the Cambridge structural database (Allen *et al.* 1991), equations (4.2) and (4.3) can be used to obtain coordination numbers of metals in metalloenzymes in cases where the oxidation state and metal–ligand distances are known. This approach is complementary to XAS, which provides information concerning the oxidation state of a metal atom (edge position) and the dimensions of the inner coordination sphere (from EXAFS). Also, for metalloproteins, BVSA could be used to comment on the metal–ligand distances obtained from protein crystallography, since these are rarely defined with a precision better than ±0.1 Å. The following examples illustrate how the bond valence sum can be used to determine the coordination environment of metal centres, using bond lengths obtained from the analysis of EXAFS data.

From the analysis of the Ni K-edge EXAFS obtained for the nickel site in carbon monoxide dehydrogenase from *Rhodospirillum rubrum* (Tan *et al.* 1992), the nickel was proposed to be coordinated to two S atoms at a distance of 2.22 Å, and 2–3 N atoms at a distance of 1.86 Å. The result of the bond valence sum calculation for the five-coordinate metal centre is 2.42 (Ni—N, $r_0 = 1.449$, $B = 0.57$; Ni—S, $r_0 = 1.721$, $B = 0.68$), clearly too large, indicating that the coordination number of the metal centre is too high. However, if the sum is repeated using a four-coordinate metal centre, with only two N at 1.86 Å, the oxidation state is calculated to be 1.93. A four-coordinate metal centre is in agreement with the proposed coordination environment of the nickel centre found in carbon monoxide dehydrogenase from *Clostridium thermoaceticum* (Xia *et al.* 1995; Bastian *et al.* 1988).

The crystal structure of Cd_5Zn_2 metallothionein has been reported (Braun *et al.* 1992) and the metal atoms are shown to be bound in two clusters, as Cd_4 and $CdZn_2$, with each metal being ligated by four cysteinyl sulphur atoms. EXAFS studies (Abrahams *et al.* 1986) have shown sulphur ligation at 2.51 Å for Cd and 2.33 Å for Zn. The oxidation state calculated for a four-coordinate cadmium metal centre is 2.13 (Cd—S; $r_0 = 2.215$, $B = 0.47$) and 2.01 for a four-coordinate Zn atom (Zn—S; $r_0 = 1.573$, $B = 1.10$). From the results of the calculations, it can be seen that the bond lengths derived from the EXAFS data concur with the proposed coordination environment determined by protein crystallography.

(*b*) *Distortion theorem*

The distortion theorem (Brown & Shannon 1973) states that the displacement of a metal atom from the centre of a polyhedron will result in an increase in the calculated bond valence sum (see figure 12). Therefore, the minimum value of the bond valence sum is calculated for the metal atom at the centre of a polyhedron. The distortion theorem has been applied, for example, to assess possible positions for metal sites in proteins. Gregory *et al.* (1993) proposed a method of determining the position of a metal atom within a cavity described by the ligand atoms. Once the cavity for the metal atom was established, the metal atom was placed at the centre of the cavity and the coordinates of the metal centre which minimized the

PHILOSOPHICAL TRANSACTIONS OF THE ROYAL SOCIETY A MATHEMATICAL, PHYSICAL & ENGINEERING SCIENCES

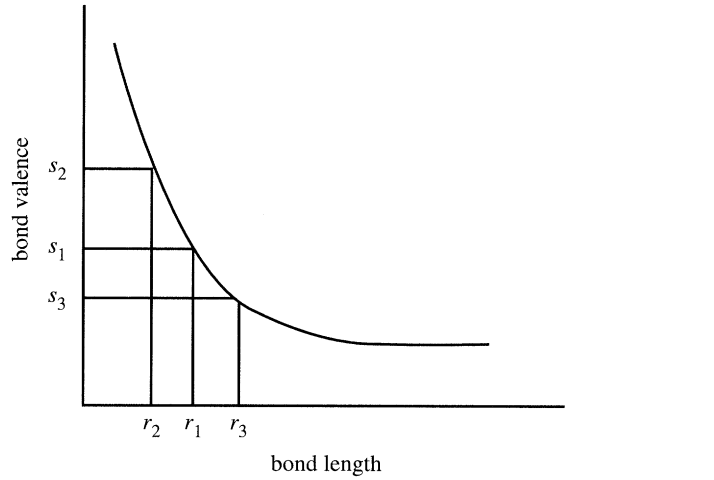

Figure 12. Diagram illustrating the effect upon the contribution to the bond valence when the metal ion, in the centre of a polyhedron, bond lengths r_1 is displaced to give shorter (r_2) and longer (r_3) bond lengths.

difference between bond lengths to the ligand atoms, and 'ideal' bond lengths, were established. The 'ideal' bond lengths for 22 cation–anion pairs were calculated from the examination of 28 metal centres in macromolecules, as determined by protein crystallography.

As a refinement of this procedure, we propose an approach which permits the position of a metal atom to be determined upon the basis of bond valence sum calculations, combined with a 'check' on the bond lengths generated by the position of the metal atom. If the calculated bond length lies within $\pm 2\sigma$ of the mean bond length determined from the relevant cation–anion pair data set obtained from the CSD, a score of 1 is give to the bond length. If the bond lies to within $\pm(2\text{–}3)\sigma$ of the mean, the bond is given a score of 10, and if it is greater or less than the mean of the bond length $\pm 3\sigma$, the bond is accorded a score of 20. Thus, for a proposed position of the metal centre to be considered, ideally the total bond length score should be no greater than the coordination number of the metal centre.

The crystal structure of rat liver metallothionein II, has been refined to 2.0 Å, has an R factor of 0.197, and root mean square deviation (RMSD) of bond distances of 0.02 Å (Braun *et al.* 1992). The coordinates of the zinc atom (Zn(1)) in the cavity of cysteinyl sulphur ligand atoms are given in table 1, which indicates that the Zn—S(15) bond length is very short at 1.78 Å. A bond length score of 20 assigned to the short $Zn—S_{cys}$ bond indicates the bond length is not common in the Zn(II)—S data set obtained from the CSD, from which the 'ideal' bond length and the value of the standard deviation used in the scoring system had been calculated. The calculated oxidation state using $r_0 = 1.573$ Å and $B = 1.10$ for the zinc centre of 2.28 is high, also indicating that the bond lengths are, on the whole, too short. By implementing our application of the distortion theorem, it was found that there were 13 possible positions for the metal atom where each bond length obtained a score of 1, thus the overall bond length score was 4, and the calculated oxidation state was close to 2.0. The coordinates and calculated oxidation state of the five best positions for the metal atoms are given in table 2.

The position of the metal atom which has the best calculated oxidation state (2.07)

Table 1. *Coordinates of zinc and sulphur atoms in rat liver metallothionein II (Braun et al. 1992)*

	coordinates /Å			Zn—S
atom	x	y	z	bond length /Å
Zn(1)	19.064	9.879	44.575	
S(15)	20.846	9.585	44.575	1.78
S(19)	16.985	8.917	44.733	2.30
S(24)	18.987	12.263	44.237	2.41
S(29)	19.828	8.814	42.564	2.40

Table 2. *Calculated positions of the zinc atom and oxidation state for zinc in rat liver metallothionein II*

coordinates /Å			
x	y	z	oxidation state[a]
18.475	10.192	43.670	2.07
18.475	10.142	43.770	2.08
18.475	10.192	43.720	2.08
18.525	10.192	43.670	2.09
18.475	10.192	43.770	2.09

[a]Calculated from equations (4.2) and (4.3) using $r_0 = 1.573$ Å and $B = 1.10$.

Table 3. *Zn(1)—S bond lengths in rat liver metallothionein II calculated from optimized positions of the zinc atom*

	bond lengths /Å				
calculated oxidation state[a]	S(15)	S(19)	S(24)	S(29)	average
2.07	2.56	2.23	2.21	2.23	2.31
2.08	2.55	2.02	2.26	2.20	2.26
2.08	2.54	2.21	2.20	2.26	2.30
2.09	2.51	2.26	2.20	2.20	2.29
2.09	2.52	2.18	2.18	2.28	2.29

[a]Calculated from equations (4.2) and (4.3) using $r_0 = 1.573$ Å and $B = 1.10$.

is at a distance of 1.12 Å from the proposed site of the metal centre as defined from protein crystallography. Table 3 contains the bond lengths calculated for the above positions of the metal atom.

The information presented in table 3 shows that in all cases the reassessment of the

Table 4. *Coordinates of the Ni(2) atom and its ligand donor atoms of nickel urease from Klebsiella aerogenes (Jabri et al. 1995)*

	coordinates /Å			
atom	x	y	z	bond length /Å
Ni(2)	68.029	104.624	72.462	
N_{His}	66.153	103.848	73.519	2.29
N_{His}	69.398	102.926	71.984	2.23
O_{Asp}	68.830	104.623	74.420	2.12
O_{Lys}	67.048	104.244	70.596	2.14
O_{H_2O}	69.209	106.110	71.905	1.98

position of zinc within the cavity of the four sulphur atoms leads to a lengthening of the Zn—S(15) bond; indeed the position of zinc which has the closest correspondence to an oxidation state of 2.0 has the longest bond to S(15). The other Zn—S bond lengths are all shorter than the crystallographic values. The average $Zn—S_{cys}$ bond length determined crystallographically is 2.22 Å (see table 1) and the optimization of the zinc position based on bond valence sum considerations leads to a longer average Zn—S bond length (table 3). The values in table 3, notably for the best agreement between calculated and actual oxidation states, are close to the (average) value determined from the analysis of Zn K-edge EXAFS for the zinc site, of 2.33 Å (Abrahams *et al.* 1986), which leads to a calculated oxidation state of 2.01.

The crystal structure of nickel urease from *Klebsiella aerogenes* (Jabri *et al.* 1995) (see figure 5) is refined to a value of 2.2 Å, R factor of 0.182 and RMSD of bond distances of 0.008 Å. The orthogonalized coordinates of the five-coordinate nickel site (Ni(2)) in the protein are given in table 4.

The overall bond length score for the above position is 14, calculated from a comparison of bond lengths obtained from the CSD, and three of the bond lengths are very close to the upper limit of the 96% level of acceptability and, therefore, the calculated oxidation state is low, at 1.47. Application of the distortion theorem detailed above finds 24 positions where the bond length score is 5, but three of the bond lengths remain long, and the most accurate calculation of the oxidation state is 1.51 (Ni—N, $r_0 = 1.449$, $B = 0.57$; Ni—O, $r_0 = 1.387$, $B = 0.62$), with bond lengths of (Ni—N) at 2.37 and 2.03 Å, and (Ni—O) at 2.16, 2.09 and 2.17 Å. The fact that it is not possible to find a position of the metal atom for which the oxidation state calculation is in reasonable agreement with the actual oxidation state using realistic bond lengths indicates that the cavity proposed by protein crystallography is too large for the metal atom. Thus, for an accurate calculation of oxidation state, the dimensions of the ligand cavity needs to be reduced.

Thus, the coordination environment of a metal centre in a ligand cavity proposed from protein crystallography can be examined on the basis of a comparison between calculated and the actual oxidation state. Hence, alternative sites for the location of the metal may be suggested within the cavity of the ligands. The accuracy of this approach should be improved significantly if the metal edge EXAFS measured for the same crystalline state is available to check the various metal–ligand distances proposed.

5. Conclusions

We have tried to demonstrate in this review the varied coordination chemistry of d-transition metal atoms in proteins, especially for sites of catalytic activity within enzymes. The study of these systems is clearly advancing rapidly. The synergy which is developing, by combining the results of crystallographic and spectroscopic investigations, should allow us to gain an understanding of the manner in which catalysis is achieved and controlled at transition metal centres in enzymes.

Herein, we have presented a selective review of advances made in the characterization of d-transition metal centres in proteins by crystallography and X-ray absorption spectroscopy. Furthermore, we advocate the use of BVSA, either simply or via a distortion theorem approach to inspect the structure of a d-transition metal site in protein obtained from EXAFS analysis and/or protein crystallography as an aid to good judgement, but not as a substitute for this.

We thank The Royal Society for the award of a Fellowship (D.C.) and the University of Manchester for the award of a Scholarship (E.P.).

References

Abrahams, I. L., Bremner, I., Diakun, G. P., Garner, C. D., Hasnain, S. S., Ross, I. & Vasak, M. 1986 Structural studies of the copper and zinc sites in metallothioneins by using extended X-ray-absorption fine structure. *Biochem. J.* **236**, 585–589.

Adams, M. W. W. 1994 Tungsten proteins. In *Encyclopaedia of inorganic chemistry* (ed. R. B. King), pp. 4284–4291. New York: Wiley.

Adams, M. W. W., Mortenson, L. E. & Chen, J.-S. 1981 Hydrogenase. *Biochim. Biophys. Acta.* **594**, 105–176.

Allen, F. H., Davies, J. E., Galloy, J. J., Johnson, O., Kennard, O., Macrae, C. F., Mitchell, E. M., Mitchell, G. F., Smith, J. M. & Watson, D. G. 1991 The development of version-3 and version-4 of the Cambridge structural database system. *J. Chem. Inf. Comp. Sci.* **31**, 187–204.

Arber, J. M., Dobson, B. R., Eady, R. R., Stevens, P., Hasnain, S. S., Garner, C. D. & Smith, B. E. 1987 Vanadium *K*-edge X-ray absorption spectrum of the VFe-protein of the vanadium nitrogenase of *Azotobacter chroococcum*. *Nature* **325**, 372–374.

Arber, J. M., Flood, A. C., Garner, C. D., Gormal, C. A., Hasnain, S. S. & Smith, B. E. 1988 Iron *K*-edge X-ray absorption spectroscopy of the iron-molybdenum cofactor of the nitrogenase from *Klebsiella pneumoniae*. *Biochem. J.* **252**, 421–425.

Baker, E. N. 1988 The structure of azurin from *alicaligenes denitrificans*: refinement at 1.8 Å resolution and comparison of the two crystallographically independent molecules. *J. Molec. Biol.* **203**, 1071–1095.

Barondeau, D. P., Roberts, L. M. & Lindahl, P. A. 1994 Stability of the Ni–C state and oxidative titrations of *Desulfovibrio gigas* hydrogenase monitored by EPR and electronic absorption spectroscopies. *J. Am. Chem. Soc.* **116**, 3442–3448.

Bastian, N. R., Diekert, G., Niederhoffer, E. C., Teo, B.-K., Walsh, C. T. & Orme-Johnson, W. H. 1988 Nickel and iron EXAFS of carbon monoxide dehydrogenase from *Clostridium thermoaceticum*, strain DSM. *J. Am. Chem. Soc.* **110**, 5581–5582.

Bergerhoff, G., Hundt, R., Sievers, R. & Brown, I. D. 1983 The inorganic crystal structure database. *J. Chem. Inf. Comp. Sci.* **23**, 66–69.

Blackburn, N. J., Hasnain, S. S., Binsted, N., Diakun, G. P., Garner, C. D. & Knowles, P. F. 1984 X-ray absorption fine structure of bovine erythrocyte superoxide dismutase in aqueous solution; direct evidence for a three-coordinate Cu(I) in the reduced enzyme. *Biochem. J.* **219**, 985–990.

Bolin, J. T., Ronco, A. E., Morgan, T. V., Mortenson, L. E. & Xuong, N.-H. 1993 The unusual metal-clusters of nitrogenase: structural features revealed by X-ray anomalous diffraction

studies of the MoFe-protein from *Clostridium pasteurianum*. *Proc. Natn. Acad. Sci. U.S.A.* **90**, 1078–1082.

Braun, W., Vasak, M., Robbins, A. H., Stout, C. D., Wagner, G., Kagi, J. H. R. & Wuthrich, K. 1992 Comparison of the NMR solution structure and the X-ray crystal structure of rat metallothionein II. *Proc. Natn. Acad. Sci. U.S.A.* **89**, 10 124–10 128.

Bray, R. C. 1988 The inorganic biochemistry of molybdoenzymes. *Q. Rev. Biophys.* **21**, 299–329.

Brown, I. D. & Altermatt, D. 1985 Bond-valance parameters obtained from a systematic analysis of the inorganic crystal structure database. *Acta. Crystallogr.* B **41**, 244–247.

Brown, I. D. & Shannon, R. D. 1973 Empirical bond-strength–bond-length curves for oxides. *Acta Crystallogr.* A **29**, 266–282.

Commack, R., Patil, D. S., Hatchikian, E. C., Fernandez, V. M. 1987 Nickel and iron-sulfur centres in *desulfovibrio-gigas* hydrogenase—electron spin resonance spectra, redox properties and interactions. *Biochim. Biophys. Acta* **912**, 98–109.

Chan, M. K., Kim, J. S. & Rees, D. C. 1993 The nitrogenase FeMo-cofactor and P cluster pair: 2.2 Å resolution structure. *Science* **260**, 792–794.

Chan, M. K., Mukund, S., Kletzin, A., Adams, M. W. W. & Rees, D. C. 1995 Structure of a hyperthermophilic tungstopterin enzyme, aldehyde ferredoxin oxidoreductase. *Science* **267**, 1463–1469.

Charnock, J. M., Garner, C. D., Abrahams, I. L., Arber, J. M., Hasnain, S. S., Henehan, C. & Vasak, M. 1989 EXAFS study of metallothionein. *Physica* **158B**, 93–94.

Colby, J., Stirling, D. I. & Dalton, H. 1977 The soluble methane monooxygenase of *Methylococcus capsulatus* (Bath). *J. Molec. Biol.* **227**, 283–285.

Conradson, S. D., Burgess, B. K., Newton, W. E., Mortenson, L. E. & Hodgson, K. O. 1987 Structural studies of the molybdenum site in the MoFe protein and its FeMo cofactor by EXAFS. *J. Am. Chem. Soc.* **109**, 7507–7515.

Cramer, S. P. & Hodgson, K. O. 1979 X-ray absorption spectroscopy: a new structural method and its application to bioinorganic chemistry. *Prog. Inorg. Chem.* **25**, 1–39.

Cramer, S. P., Gillum, W. O., Hodgson, K. O., Mortenson, L. E., Stiefel, E. I., Chisnell, J. R., Brill, W. J. & Shah, V. K. 1978*a* The molybdenum site of nitrogenase 2. A comparative study of Mo-Fe proteins and the iron–molybdenum cofactor by X-ray absorption spectroscopy. *J. Am. Chem. Soc.* **100**, 3814–3819.

Cramer, S. P., Hodgson, K. O., Gillum, W. O. & Mortenson, L. E. 1978*b* The molybdenum site of nitrogenase. Preliminary structural evidence from X-ray absorption spectroscopy. *J. Am. Chem. Soc.* **100**, 3398–3407.

Cramer, S. R. & Hille R. 1985 Arsenite-inhibited xanthine oxidase: determination of the Mo–S–As geometry by EXAFS. *J. Am. Chem. Soc.* **107**, 8164–8169.

da Silva, J. J. R., Fraústo & Williams, R. J. P. 1991 *The biological chemistry of the elements: the inorganic chemistry of life*. Oxford: Clarendon.

Dancis, A., Yuan, D. S., Haile, D., Askwith, C., Eide, D., Moehle, C., Kaplan, J. & Klausner, R. R. 1994 Molecular characterisation of a copper transport protein in *Saccharomyces cerevisiae*: an unexpected role for copper in iron transport. *Cell* **76**, 393–402.

DeRose, V. J., Liu, K. E., Kurtz, D. M. Jr, Hoffman, B. M. & Lippard, S. J. 1993 Proton ENDOR identification of bridging hydroxide ligands in mixed-valent diiron centres of proteins: methane monoxygenase and semimet azidohemerythrin. *J. Am. Chem. Soc.* **115**, 6440–6441.

DeWitt, J. G., Rosenzweig, A. C., Hedman, B., Lippard, S. J. & Hodgson, K. O. 1995 X-ray absorption spectroscopic studies of the diiron centre in methane monooxygenase in the presence of substrate and coupling protein of the enzyme system. *Inorg. Chem.* **34**, 2505–2515.

Dixon, N. E., Gazzola, C., Blackeley, R. L. & Zerner, B. 1975 Jack bean urease (EC 3.5.1.5). A metalloenzyme. A simple biological role for nickel? *J. Am. Chem. Soc.* **97**, 4131–4133.

Dixon, N. E., Riddles, P. W. Gazzola, C., Blackeley, R. L. & Zerner, B. 1980 Jack bean urease (EC 3.5.1.5). V. On the mechanism of urease on urea, formamide, acetamide, N-methyl urea and related compounds. *Can. J. Biochem.* **58**, 1335–1344.

Douglas, T., Dickson, D. P. E., Betteridge, S., Charnock, J. M., Garner, C. D. & Mann, S. 1995 Synthesis and structure of an iron(III) sulfide-ferritin bioinorganic nanocomposite. *Science* **269**, 54–57.

PHILOSOPHICAL TRANSACTIONS OF THE ROYAL SOCIETY A MATHEMATICAL, PHYSICAL & ENGINEERING SCIENCES

Drennan, C. L., Huang, S., Drummond, J. T. Matthews, R. G. & Ludwig, M. L. 1995 How a protein binds B12: a 3.0 Å X-ray structure of B_{12}-binding domains of methionine synthase. *Science* **266**, 1669–1674.

Duine, J. A. & Jongejan, J. A. 1989 Quinoproteins, enzymes with pyrroloquinoline quinone as cofactor. *A. Rev. Biochem.* **58**, 403–426.

Eady, R. R. 1995 Vanadium nitrogenases of azotobacter. In *Metal ions in biological systems: vanadium and its role in life* (ed. H. Sigel & A. Sigel), vol. 31, pp. 363–405. New York: Marcel Dekker.

Farnum, M., Palcic, M. & Klinman, J. P. 1986 pH-dependence of deuterium-isotope effects and tritium exchange in the bovine plasma amine oxidase—a role for single-base catalysis in amine oxidation and imine exchange. *Biochem.* **25**, 1898–1904.

Ford, G. C., Harrison, P. M., Rice, D. W., Smith, J. M. A., Treffry, A., White, J. L. & Yariv, J. 1984 Ferritin: design and formation of an iron-storage protein. *Phil. Trans. R. Soc. Lond.* B **304**, 551–565.

Garner, C. D. 1991 X-ray absorption spectroscopy and the structures of transition metal centres in proteins. *Adv. Inorg. Chem.* **36**, 303–339.

George, G. N., Coyle, C. L., Hales, B. J. & Cramer, S. P. 1988 X-ray absorption of *Azotobacter vinelandii* vanadium nitrogenase. *J. Am. Chem. Soc.* **110**, 4057–4059.

George, G. N., Kipke, C. A., Prince, R. C., Sunde, R. A., Enemark, J. H. & Cramer, S. P. 1989 Structure of the active site of sulfite oxidase: X-ray absorption spectroscopy of Mo(IV), Mo(V), and Mo(VI) oxidation states. *Biochem.* **28**, 5075–5080.

George, G. N., Prince, R. C., Mukund, S. & Adams, M. W. W. 1992 Aldehyde ferredoxin oxidoreductase from the hyperthermophilic archaebacterium *pyrococcus-furiosus* contains a tungsten oxo-thiolate centre. *J. Am. Chem. Soc.* **114**, 3521–3523.

Godden, J. W., Turley, S., Teller, D. C., Adman, E. T., Liu, M. Y., Payne, W. J. & LeGall, J. 1991 The 2.3 Å X-ray structure of nitrite reductase from *Achromobacter cycloclastes. Science* **253**, 438–442.

Gregory, D. S., Martin, A. C. R., Cheetham, J. C. & Rees, A. R. 1993 The prediction and characterisation of metal sites in proteins. *Protein Engng* **6**, 29–35.

Halpern, J. 1982 *B_{12} chemistry* (ed. D. Dolphin), vol. 1, pp. 501-541. New York: Wiley.

Harvey, I., Arber, J. M., Eady, R. R., Smith, B. E., Garner, C. D. & Hasnain, S. S. 1990 Iron *K*-edge X-ray absorption spectroscopy of the iron–vanadium cofactor of the vanadium nitrogenase from *Azotobacter chroococcum. Biochem. J.* **266**, 929–931.

Heath, S. L., Charnock, J. M., Garner, C. D. & Powell, A. K. 1996 Extended X-ray absorption fine structure (EXAFS) studies of oxyhydroxide aggregates and a critique of their use as models for ferritin. *Chem. Int. J.* (In the press.)

Hedman, B., Hodgson, K. O. & Garner, C. D. 1990 Characterisation of molybdenum and vanadium centres in enzymes by X-ray absorption spectroscopy. In *Synchrotron radiation and biophysics* (ed. S. S. Hasnain), pp. 43–62. Chichester: Ellis Horwood.

Hodgkin, D. C., Kamper, J., Mackay, M. & Pickworth, J. 1956 Structure of vitamin B_{12}. *Nature* **178**, 64–66.

Holmes, M. A., Le Trong, I., Turley, S., Sieker, L. C. & Stenkamp, R. E. 1991 The structures of deoxy and oxy hemerythrin at 2.0 Å resolution. *J. Molec. Biol.* **218**, 583–593.

Islam, Q. T., Sayers, D. E., Gorun, S. M. & Theil, E. C. 1989 A comparison of an undecairon(III) complex with the ferritin iron core. *J. Inorg. Biochem.* **36**, 51–62.

Jabri, E., Carr, M. B., Hausinger, R. P. & Karplus, P. A. 1995 The crystal structure of urease from *Klebsiella aerogenes. Science* **268**, 998–1004.

Janes, S. M., Mu, D., Wemmer, D., Smith, A. J., Kaur, S., Maltby, D., Burlingame, A. L. & Klinman, J. P. 1990 A new redox cofactor in eukaryotic enzymes; 6-hydroxydopa at the active site of bovine serum amine oxidase. *Science* **248**, 981–987.

Johnson, J. L., Bastian, N. R. & Rajagopalan, K. V. 1990 Molybdopterin guanine dinucleotide—a modified form of molybdopterin identified in the molybdenum cofactor of dimethyl sulfoxide reductase from *Rhodobacter sphaeroides forma specialis denitrificans. Proc. Natn. Acad. Sci. U.S.A.* **87**, 3190–3194.

PHILOSOPHICAL TRANSACTIONS OF THE ROYAL SOCIETY A MATHEMATICAL, PHYSICAL & ENGINEERING SCIENCES

Karrasch, M., Borner, G. & Thauer, R. K. 1990 The molybdenum cofactor of formylmethanofuran dehydrogenase from *Methanosarcina barkeri* is a molybdopterin guanine dinucleotide. *FEBS Lett.* **274**, 48–52.

Kim, E. E. & Wyckoff, H. W. 1991 Reaction mechanism of alkaline-phosphatase based on crystal structure: 2, metal ion catalysis. *J. Molec. Biol.* **218**, 449–464.

Kim, J. S. & Rees, D. C. 1992 Structural models for the metal centres in the nitrogenase molybdenum-iron protein. *Science* **257**, 1677–1682.

Kincaid, B. M. & Eisenberger, P. 1975 Synchrotron radiation studies of the K-edge photoabsorption spectra of krypton, bromine, and germanium tetrachloride. Comparison of theory and experiment. *Phys Rev. Lett.* **34**, 1361–1364.

Klinman, J. P. & Mu, D. 1994 Quinoenzymes in biology. *A. Rev. Biochem.* **63**, 299–344.

Labhardt, A. & Yuen, C. 1979 X-ray absorption edge fine structure spectroscopy of the active site heme of cytochrome c. *Nature* **277**, 150–151.

Lee, S.-K., Nesheim, J. C. & Lipscomb, J. D. 1993 Transient intermediates of the methane monooxygenase catalytic cycle. *J. Biol. Chem.* **268**, 21 569–21 577.

Lippard, S. J. 1995 At last—the crystal structure of urease. *Science* **268**, 996–997.

Lipscomb, J. D. 1994 Biochemistry of the soluble methane monooxygenase. *A. Rev. Microbiol.* **48**, 371–399.

Liu, H. I., Filipponi, A., Gavini, N., Burgess, B. K., Hedman, B., Di Ciccio, A., Natoli, C. R. & Hodgson, K. O. 1994 EXAFS studies of FeMo-cofactor and MoFe protein: direct evidence for the long range Mo–Fe–Fe interaction and cyanide binding to the Mo in FeMo-cofactor. *J. Am. Chem. Soc.* **116**, 2418–2423.

Liu, K. E. & Lippard, S. J. 1995 Characterization of a diiron(III) peroxo intermediate in the reaction cycle of methane monooxygenase hydroxylase from *Methylococcus capsulatus* (Bath). *J. Am. Chem. Soc.* **117**, 4987–4990.

Liu, K. E., Johnson, C. C., Newcomb, M. & Lippard, S. J. 1993 Radical clock studies and kinetic isotope effect studies of the hydroxylation of hydrocarbons by methane monooxygenase. *J. Am. Chem. Soc.* **115**, 939–947.

Mackle, P., Charnock, J. M., Garner, C. D., Meldrum, F. C., Mann, S. 1993 Characterisation of the manganese core of reconstituted ferritin by X-ray absorption spectroscopy. *J. Am. Chem. Soc.* **115**, 8471–8472.

Mackle, P., Garner, C. D., Ward, R. J. & Peters, T. J. 1991 Iron K-edge absorption spectroscopy investigations of the cores of ferritin and haemosiderins. *Biochem. Biophys. Acta.* **1116**, 145–150.

Meldrum, F. C., Wade, V. J., Nimmo, D. L., Heywood, B. R. & Mann, S. 1991 Synthesis of inorganic nanophase materials in supramolecular protein cages. *Nature* **349**, 684–687.

Messerschmidt, A., Landenstein, R., Huber, R., Bolognesi, M., Avigliano, L., Petruzzelli, R., Rossi, A. & Finazzi-Agró, A., 1992 Refined crystal structure of ascorbate oxidase at 1.9 Å resolution. *J. Molec. Biol.* **224**, 179–205.

Mu, D., Janes, S. M., Smith, A. J., Brown, D. E., Dooley, D. M. & Klinman, J. P. 1992 Tyrosine codon corresponding to topa quinone at the active-site of copper amine oxidases. *J. Biol. Chem.* **267**, 7979–7982.

Nar, H., Messerschmidt, A., Huber, R., van der Kamp, M. & Canters, G. W. 1991 Crystal structure analysis of oxidized *Pseudomonas aeruginosa* azurin at pH 5.5 and 9.6: a pH-induced conformation transition involves a peptide-bond flip. *J. Molec. Biol.* **221**, 765–772.

Nordlund, P., Sjöberg, B.-M. & Eklund, H. 1990 3-Dimensional structure of the free-radical protein of ribonucleotide reductase. *Nature* **345**, 593–598.

Ono, T., Noguchi, T., Inune, Y., Kusunoki, M., Yamaguchi, H. & Oyanagi, H. 1995 XANES spectroscopy for monitoring intermediate reaction states of Cl^--depleted Mn cluster in photosynthetic water oxidation centre. *J. Am. Chem. Soc.* **117**, 6386–6387.

Pang, C.-P., Chakravarti, B., Adington, R. M., Ting, H. H., White, R. L., Jayatilake, G. S., Baldwin, J. E. & Abraham, E. P. 1984 Purification of isopenicillin N synthase. *Biochem. J.* **222**, 789–795.

Park, I.-S. & Hausinger, R. P. 1995 Requirement of carbon dioxide for *in vitro* assembly of the urease metallo centre. *Science* **267**, 1156–1158.

PHILOSOPHICAL TRANSACTIONS OF THE ROYAL SOCIETY A MATHEMATICAL, PHYSICAL & ENGINEERING SCIENCES

Parsons, M. R., Covery, M. A., Wilmot, C. M., Yadav, K. D. S., Blakeley, V., Corner, A. S., Phillips, S. E. V., McPherson, M. J. & Knowles, P. F. 1995 Crystal structure of a quinoenzyme: copper amine oxidase of *Escherichia coli* at 2 Å resolution. *Structure* **3**, 1171–1184.

Pauling, L. 1929 The principles determining the structure of complex ionic crystals. *J. Am. Chem. Soc.* **51**, 1010–1026.

Pidcock, E., Collison, D. & Garner, C. D. 1993 The bond valence sum approach to the determination of structure at metal centres in biological systems. *J. Inorg. Biochem.* **51**, 173.

Powell, A. K., Heath, S. L., Gatteschi, D., Pardi, L., Sessoli, R., Spina, G., Del Giallo, F. & Pieralli, F. 1995 Synthesis, structures, and magnetic properties of Fe_2, Fe_{17}, and Fe_{19} oxo-bridged iron clusters: the stabilisation of high ground state spins by cluster aggregates. *J. Am. Chem. Soc.* **117**, 2491–2502.

Powers, L. 1982 X-ray absorption spectroscopy: application to biological molecules. *Biochim. Biophys. Acta.* **683**, 1–38.

Priggemeyer, S., Eggersborkenstein, P., Ahlers, F., Henkel, G., Korner, M., Witzel, H., Nolting, H. F., Hermes, C. & Krebs, B. 1995 XAS investigations on the iron–zinc center of purple acid phosphatase from red kidney beans. *Inorg. Chem.* **34**, 1445–1454.

Rajagopalan, K. V. 1991 Novel aspects of the biochemistry of the molybdenum cofactor. *Adv. Enzymol. Rel. Area Molec. Biol.* **64**, 215–290.

Randall, C. R., Zang, Y., True, A. E., Que, L. Jr., Charnock, J. M., Garner, C. D., Fujishima, Y., Schofield, C. J. & Baldwin, J. E. 1993 X-ray absorption studies for the ferrous site of isopenicillin N synthase and related model compounds. *Biochem.* **32**, 6664–6673.

Rardin, R. L., Tolman, W. B. & Lippard, S. J. 1991 Monodentate carboxylate complexes and the carboxylate shift: implications for polymetalloprotein structure and function. *New. J. Chem.* **15**, 417–430.

Roach, P. L., Clifton, I. J., Fülöp, V., Harlos, K., Barton, G. J., Hajdu, J., Andersson, I., Schofield., C. J. & Baldwin, J. E. 1995 Crystal structure of isopenicillin N synthase is the first from a new structural family of enzymes. *Nature* **375**, 700–704.

Rosenzweig, A. C. & Lippard, S. J. 1994 Determining the structure of a hydroxylase enzyme that catalyzes the conversion of methane to methanol in methanotrophic bacteria. *Acc. Chem. Res.* **27**, 229–236.

Rosenzweig, A. C., Frederick, C. A., Lippard, S. J. & Nordlund, P. 1993 Crystal structure of a bacterial non-haem iron hydroxylase that catalyses the biological oxidation of methane. *Nature* **366**, 537–543.

Rosenzweig, A. C., Nordlund, P., Takahara, P. M., Frederick, C. A. & Lippard, S. J. 1995 Geometry of the soluble methane monooxygenase catalytic diiron center in two oxidation states. *Chem. Biol.* **2**, 409–418.

Scott, R. A. 1985 Measurement of metal–ligand distances by EXAFS. *Meth. Enzym.* **117**, 414–459.

Shulman, R. G., Eisenberger, P., Teo, B. K., Kincaid, B. M. & Brown, G. S. 1978 Fluorescence X-ray absorption studies of rubredoxin and its model compounds. *J. Molec. Biol.* **124**, 305–321.

Smith, W. W., Burnett, R. M., Darling, G. D. & Ludwig, M. L. 1977 Structure of the semiquinone form of flavodoxin from *Clostridium MP*. Extension of 1.8 Å resolution and some comparisons with the oxidized state. *J. Molec. Biol.* **117**, 195–225.

Stiefel, E. I., Coucouvanis, D. & Newton, W. E. 1993 *Molybdenum Enzymes, Cofactors, and Model Systems* (ACS Symposium Series 535). Washington, DC: American Chemistry Society.

Sträter, N., Klabunde, T., Tucker, P., Witzel, H. & Krebs, B. 1995 Crystal structure of a purple acid phosphatase containing a dinuclear Fe(III)–Zn(II) active site. *Science* **268**, 1489–1492.

Stubbe, J. 1995 Binding site revealed of Nature's most beautiful cofactor. *Science* **266**, 1663–1664.

Suerbaum, H., Korner, M., Witzel, H., Althaus, E. & Mosel, B. D. 1993 Zn-exchange and Mössbauer studies on the [Fe–Fe] derivatives of the purple acid phosphatase from kidney beans. *Eur. J. Biochem.* **214**, 313–321.

Sumner, J. B. 1926 The recrystallisation of urease. *J. Biol. Chem.* **70**, 97–98.

PHILOSOPHICAL TRANSACTIONS OF THE ROYAL SOCIETY A MATHEMATICAL, PHYSICAL & ENGINEERING SCIENCES

Takahashi, N., Ortel, T. L. & Putnam, F. W. 1984 Single-chain structure of human ceruloplasmin: the complete amino-acid sequence of the whole molecule. *Proc. Natn. Acad. Sci. U.S.A.* **81**, 390–394.

Tan, G. O., Ensign, S. A., Ciurli, S., Scott, M. J., Hedman, B., Holm, R. H., Ludden, P. W., Karszun, Z. R., Stephens, P. J. & Hodgson, K. O. 1992 On the structure of the Nickel–iron–sulphur center of the carbon monoxide dehydrogenase from *Rhodospirillum rubrum* an X-ray absorption spectroscopy study. *Proc. Natn. Acad. Sci. U.S.A.* **89**, 4427–4431.

Teixeira, M., Moura, I., Xavier, A. V., Moura, J. J. G., LeGall, J., Devartanian, D. V., Peck, H. d. & Huynh, B. H. 1989 Redox intermediates of *Desulfovibrio gigas* [NiFe] hydrogenase generated under hydrogen: Mössbauer and EPR characterization of their metal centers. *J. Biol. Chem.* **264**, 16 435–16 450.

Turner, N. A., Bray, R. C. & Diakun, G. P. 1989 Information from EXAFS spectroscopy on the structures of different forms of molybdenum in xanthine oxidase and the catalytic mechanism of the enzyme. *Biochem. J.* **260**, 563–571.

van der Zwaan, Albracht, S. P. J., Fontijn, R. D. & Slater, E. C., 1985 Monovalent nickel in hydrogenase from *Chromatium vinosum*: light sensitivity and evidence for direct interaction with hydrogen. *FEBS Lett.* **179**, 271–277.

Vincent, J. B., Olivier-Lilley, G. L. & Averill, B. A. 1991 Proteins containing oxo-bridged dinuclear iron centres: a bioinorganic perspective. *Chem. Rev.* **90**, 1447–1467.

Volbeda, A., Charon, M.-H., Piras, C., Hatchikian, E. C., Frey, M. & Fontecilla-Camps, J. C. 1995 Crystal structure of the nickel-iron hydrogenase from *Desulfovibrio gigas*. *Nature* **373**, 580–587.

Xia, J., Dong, J., Wang, S., Scott, R. A. & Lindahl, P. A. 1995 EXAFS, EPR, and electronic absorption spectroscopic study of the α metallosubunit of CO dehydrogenase from *Clostridium thermoaceticum*. *J. Am. Chem. Soc.* **117**, 7065–7070.

Yachandra, V. K., DeRose, V. J., Latimer, M. J., Mukerji, I., Sauer, K. & Klein, M. P. 1993 Where plants make oxygen: a structural model for the photosynthetic oxygen-evolving manganese cluster. *Science* **260**, 675–679.

Zaitseva, I., Zaitsev, V., Card, G., Moshkov, K., Bax, B., Ralph, A. & Lindley, P. 1996 The nature of the copper centres in human ceruloplasmin. *J. Biol. Inorg. Chem.* (In the press.)

PHILOSOPHICAL TRANSACTIONS OF THE ROYAL SOCIETY A MATHEMATICAL, PHYSICAL & ENGINEERING SCIENCES